CLEARING UP THE CAUSES OF CORNEAL CLOUDING IN ANIRIDIA-RELATED KERATOPATHY

By

DIANA K. SCAVUZZO

(under the Direction of James D. Lauderdale)

ABSTRACT

Aniridia is a rare yet visually detrimental condition, primarily caused by a heterozygous null mutation in the master regulator gene Pax6. Among other symptoms, aniridia often results in progressive corneal clouding, called aniridia-related keratopathy. This work outlines the current hypotheses as to the causes of corneal clouding and aims to address a few of these hypotheses through clinical, histological, and immunofluorescent evaluation of aniridic corneas in a mouse model. Through clinical evaluation, we characterize features of the aniridic cornea before and after the onset of aniridia-related keratopathy. Through histological evaluation, we show the correlation of conjunctivalization to corneal clouding. Through immunofluorescent evaluation, we demonstrate the presence of markers of inflammation and fibrosis. All of these techniques provide a clearer picture of what is clouding up the cornea in aniridia-related keratopathy.

INDEX WORDS: aniridia, keratopathy, aniridia-related keratopathy, cornea, corneal clouding, fibrosis, inflammation, wound healing, Pax6, cellular biology

CLEARING UP THE CAUSES OF CORNEAL CLOUDING IN ANIRIDIA-RELATED KERATOPATHY

By

DIANA K. SCAVUZZO

B.S., University of North Georgia, 2017

A Thesis Submitted to the Graduate Faculty of The University of Georgia in Partial Fulfillment of the Requirements for the Degree

MASTER OF SCIENCE

ATHENS, GEORGIA

2021

CLEARING UP THE CAUSES OF CORNEAL CLOUDING IN ANIRIDIA-RELATED KERATOPATHY

By

DIANA K. SCAVUZZO

Major Professor: James D. Lauderdale

Committee: Jonathan Eggenschwiler

Deloris Hesse

Electronic Version Approved:

Ron Walcott

Dean of the Graduate School

The University of Georgia

December 2021

DEDICATION

This thesis is dedicated to the thousands of people who suffer from aniridia, as well as their loved ones. My work is a small drop in the ocean of research devoted to finding answers for you, but I hope it can help contribute in some small way. I hope to continue helping you from the clinic in the future!

ACKNOWLEDGEMENTS

First, I would like the acknowledge the staff at the University of Georgia Coverdell Rodent Vivarium, especially our technicians Hannah Rose and Ethan Karstedt. I would also like to specifically acknowledge the leadership of Lynette Rowe and Lisa Wilson. These individuals, along with the entire CRV staff, put an incredible amount of care into their work, and our mouse colony couldn't have been in better hands. My personal thanks for your hard work and dedication.

Next, I would like to express my gratitude to my fellow graduate students and colleagues in the Lauderdale lab. Each of them has helped me in my growth as a scientist and a critical thinker. Scientific research thrives on a collaborative and open environment, and my colleagues in the Lauderdale lab helped me thrive as a scientist through thoughtful discussions and creative brainstorming sessions. It has been an honor to learn and grow alongside each of them. I am looking forward to seeing their continued success in their academic careers.

Last, but not least, I would like the acknowledge my mentors: my Major Professor James Lauderdale and my committee members Jonathan Eggenschwiler and Deloris Hesse. Dr. Lauderdale is a mentor that genuinely cares about supporting his graduate students' individual academic and career goals. He was essential in pushing me out of my comfort zone in order to help me grow in my understanding. Dr. Eggenschwiler and Dr. Hesse were greatly supportive of my goals for my project. Their thought-provoking questions and suggestions helped shape this thesis into its final form. I am grateful for their support and kindness.

TABLE OF CONTENTS

LIST OF TABLES

LIST OF FIGURES

CHAPTER 1

INTRODUCTION AND LITERATURE REVIEW

1.1 Introduction

The cornea is a transparent, avascular, dome-shaped structure making up the anterior most portion of the eye. Along with the sclera, or white of the eye, and the conjunctiva, the thin mucus-producing membrane covering the sclera, the cornea helps makes up the outer surface of the eye[1]. The cornea consists of epithelium, basement membrane, stroma, Descemet's membrane, and endothelium from anterior to posterior. Each of these layers plays a role in the cornea's primary functions, by providing protection from foreign objects, allowing the tear film to evenly distribute, and refracting light to achieve proper visual acuity[1]. The cornea is an important refractive component of the eye, at approximately 40 diopters, or 2/3rd of the refractive power[1].

The corneal epithelium is maintained by a population of stem cells located at the corneal-scleral junction, also known as the limbus. Limbal epithelial stem cells proliferate to create transient amplifying cells[1,2,6]. These transient amplifying cells migrate from the limbus at the periphery of the cornea to populate the basal layer of epithelial cells[6]. Transient amplifying cells, also known as basal epithelial cells, proliferate and migrate anteriorly to supply subsequent layers of corneal epithelium[6]. The epithelium regenerates approximately every 7-10 days, as cells are constantly sloughed off and replaced[1]. Hence, homeostasis of the corneal epithelium is achieved through proliferation of limbal stem cells, centripetal migration of transient amplifying cells, and proliferation of transient amplifying cells making up the basal layer of epithelium[7] .

The cornea achieves transparency through arrangement of collagen fibrils. Fibrils in the corneal stroma are approximately 30 nanometers in diameter, and these fibrils are spaced in a hexagonal pattern about 65 nanometers apart[5] . Fibrils form layers called lamellae that stack on top of each other in antiparallel arrangement[1,5] . These features of stromal collagen keep the cornea transparent. Several factors can lead to a loss in transparency in the cornea.

Trauma, surgery, and infection have been shown to lead to a loss in transparency of the cornea. When the cornea is wounded, it can typically heal itself within several days if solely the epithelium is damaged[1,2]. If deeper damage occurs that penetrates the epithelial basement membrane, the corneal wound healing response via maturation of fibroblasts is triggered[8]. Once they reach maturity, fibroblasts deposit disordered extracellular matrix components such as collagen type I and III[12,13]. These disordered collagens disrupt transparency, causing corneal haze, also referred to as corneal scarring, corneal clouding, or corneal fibrosis. Corneal fibrosis can take months to years to fully resolve.

Aniridia is a congenital disorder primarily caused by a mutation in the master regulator *PAX6* gene[18,21]. Aniridia causes pan-ocular changes in the structures of the eye, including iris hypoplasia, foveal hypoplasia, lens opacification, and corneal abnormalities[18]. Individuals with aniridia experience progressive corneal opacification, termed aniridia-related keratopathy (ARK)[28]. ARK is characterized by progressive neovascularization, ulceration, and infiltration of conjunctival epithelial cells, called conjunctivalization[21,28]. There are treatment methods for ARK currently available in the form of corneal and limbal transplantation, but these methods are not effective long-term[28,37] . Further research is needed to explore the source of corneal clouding in ARK in order to expand treatment options for aniridic patients.

Limbal stem cell deficiency is the predominant hypothesis for the cause of corneal fibrosis seen in ARK[21,28]. Changes in limbal architecture have been shown to correlate with conjunctivalization in aniridic patients[34]. However, the limbal stem cell population has not been directly studied as reliable markers have not yet been identified. The hypothesis proposes that the limbal stem cell population in patients with aniridia is either deficient in its ability to proliferate, or the population is decreased, causing conjunctival and vascular tissue to invade the cornea over time to compensate for epithelial cell loss. Conjunctival epithelial cells and vascular tissue are less transparent than native corneal tissue, causing a reduction in corneal transparency. With a lack of limbal stem cell markers and treatment options that target limbal stem cells, investigating other potential sources of corneal fibrosis in patients with aniridia is necessary.

The current study aims to investigate a few hypotheses of contributions to corneal clouding in ARK in a mouse model. A heterozygous null mutation in the *Pax6* gene in mice results in a strain known as *Small eye* (*Sey*), which has been shown to mimic structural changes seen in human aniridia. Using the *Sey* mouse model, mice will be investigated at time points that capture mild ARK symptoms (17-19 weeks old) and severe ARK symptoms (40+ weeks old). Clinical evaluation will be performed, and ocular surface integrity will be assessed through fluorescein uptake. Fluorescein dye is used as a marker of epithelial cell damage. Histological evaluation will be used to visualize morphological changes in the cornea as ARK symptoms progress. Conjunctival epithelial cells will be histologically evaluated as a measure of conjunctivalization, to assess whether conjunctivalization correlates with progression of ARK. Using immunofluorescence, the pro-fibrotic response will be investigated for the first time in *Sey* mice, using a myofibroblast marker (α-SMA) and a corneal wound healing marker (collagen type III).

1.2 The Cornea

When light is first incident on our eyes, it initially strikes a transparent, dome-like structure. This structure is called the cornea, and it plays an integral part in keeping our vision clear and the inner structures of our eyes protected.

The cornea, along with the sclera, makes up the outer surface of the eye. It is situated on the anterior surface of the eye, covering the iris, pupil, and other anterior chamber structures, with an average horizontal diameter of about 11 millimeters[1]. This structure is transparent, dome-shaped, and avascular. The cornea is quite thin, with an average central corneal thickness around 551-565 micrometers. This thickness increases about 50-75 micrometers from the center to the periphery of the cornea[1]. The cornea consists of three layers and two membranes.

From anterior to posterior, the cornea is made up of epithelium, epithelial basement membrane, stroma, Descemet's membrane, and endothelium[1] . Each of the layers of the cornea have particular characteristics and serve specific functions. The epithelium, as the most anterior layer, is in contact and interacts with the tear film to keep it evenly spread across the ocular surface[1]. This layer is several cells thick and constantly renews itself while providing protection to deeper layers of the cornea[1]. The epithelium has three types of cells that differ in their morphology; the basement layer are basal cells, which are typically cuboidal or columnar-shaped, mitotically active, and function to proliferate and gradually move more anteriorly to replace cells lost during normal regeneration[1] . Basal cells are also referred to as transient amplifying cells, as they are derived from a population of stem cells in the eye[6]. Basal cells detach from the epithelial basement membrane to become wing cells, the intermediate layer of corneal epithelium. These wing cells are named for their thin, wing-like shape, and are not capable of mitosis[1]. Wing cells further move anteriorly to form superficial cells, which

eventually desquamate[1]. The epithelial basement membrane (EBM) lies between the epithelium and stroma and consists of proteins such as laminins and nidogens. The epithelial basement membrane anchors the epithelium to the stroma, and serves an important function in wound healing that will be discussed further in future sections.

The stroma is composed of connective tissue consisting of keratocytes and collagens, and makes up the majority of the corneal thickness[1]. Keratocytes are mainly present in the anterior stroma, and are responsible for maintaining collagens in the stroma[1]. Collagen type I is the major collagen present in the stroma, with minimal amounts of collagens type III and IV additionally present. The stroma contributes to the cornea's refractive power and transparency[1]. Descemet's membrane connects the stroma to the endothelium, and aids in maintenance of hydration and entrance of nutrients to the cornea. The endothelium is a single cell layer, acting as a water pump to keep the stroma at the proper level of hydration[1]. There are several reasons why the cornea is a fascinating structure, including its avascularity and transparency, and each of these layers contribute to its important functions and unique features.

One key function of the cornea is its refractive power. The main purpose of our eyes as a whole is to refract light and allow passage of light that can be sensed by the cells of the retina. For optimal visual acuity, the cornea and lens refract the light entering the eye so that the light that is sensed by the retina will create a clear image once interpreted by the brain. While the shape of the lens is altered by the ciliary muscles to fine tune its refractive power, the majority of the eye's refractive power is provided by the cornea[1]. On average, the cornea contributes 40 diopters of refractive power, while the lens supplies 20 diopters[1]. If the eye were a microscope, the cornea would be the metaphorical course adjustment knob, while the lens is the fine adjustment knob. The refractive power of the cornea results from its curvature and its symmetry[1].

The symmetrical dome shape of the cornea allows light to be increasingly refracted from center to periphery, like a convex lens. Aberrations in symmetry or curvature can result in refractive errors such as astigmatism and keratoconus[4].

Protection is another important function that the cornea provides. The cornea creates a barrier to prevent foreign objects from entering the eye. Like the skin, the cornea has an epithelial layer that is constantly sloughing off and regenerating. The corneal epithelium has an average turnover rate of 7-10 days, one third of the average time for skin epithelial cell turnover[2,3]. If a foreign object produces a small scratch that removes the first few layers of epithelial cells, the basement epithelial cell layer is mitotically active and can divide and replenish the epithelium fairly quickly[1,2]. More severe damage to the cornea that disrupts this basement layer, such as damage that reaches the stroma, can take much longer, up to six weeks to fully heal[1].

The corneal epithelium is maintained through a population of stem cells located at the junction of the cornea and sclera, called the limbus. The corneal epithelium is about 5-7 cells thick in humans, with the basal cells being the only cell type in the epithelium that is mitotically active. Basal cells have been shown to proliferate and migrate superficially to replace the apical epithelial layers as they constantly slough off[1,2]. The most prevalent hypothesis of corneal epithelial maintenance states that the superficial layers of the epithelium are maintained by the basal cells, and the basal cells are maintained by limbal epithelial stem cells[1,2,6]. Stem cells in the limbus proliferate to generate transient amplifying cells, which migrate from the limbus toward the center of the cornea to maintain the basal epithelial cells[6]. While the hypothesis of a limbal stem cell niche is most widely recognized, there does exist an alternative hypothesis that the corneal epithelium has a small stem cell population of its own that helps maintain the cornea

under normal circumstances, while the limbal stem cells are only active during times of injury[6]. However, the limbal stem cell hypothesis remains the preferred explanation for corneal epithelial maintenance.

Stem cell and basal/transient amplifying cell activity increases during times of injury, as outlined by the X, Y, Z hypothesis[7]. As proposed by Thoft and Friend, corneal maintenance is represented by a simple equation: X+Y=Z, where X is the mitotic activity of basal cells, Y is the migration of cells from the limbus, and Z is the loss of epithelial cells. Therefore, when the cornea is injured and epithelial cell loss is increased, either proliferation of basal cells or cell movement from the limbus, or some combination of both, would have to increase to compensate for this cell loss[7].

A unique feature of the cornea is its transparency. This feature is an important aspect of the cornea's refractive function, as light cannot properly enter the eye without transparency. Most of the layers and membranes of the cornea are only one cell layer thick, so they do not influence its transparent nature[5]. The two main layers of the cornea that contribute to its thickness are the epithelium and the stroma. The cells of the epithelium have a homogenous refractive index, which aids in transparency[5]. Stromal transparency is most crucial, as it makes up a majority of the cornea's thickness. Transparency in the stroma is achieved through particular layering of corneal stromal fibrils, which are bundles of fibers composed of collagens, primarily collagen type I[1,5].

First, collagen fibrils have to be narrow to achieve transparency. These fibrils have a diameter of about 30 nanometers, and are regularly spaced about 65 nanometers apart[5]. Fibrils pack together and interweave to make layers called lamellae[1,5]. Hundreds of lamellae stack on top of each other with their fibers running antiparallel to the layer next to them[5]. These features

of specific diameter, spacing, and layering of corneal stromal fibrils, along with the homogenous refractive index of corneal epithelial cells, and thinness of additional layers, all keep the cornea crystal clear.

In the developing embryo, different layers of the cornea derive from multiple sources. During eye development, the neural ectoderm forms optic vesicles that extend toward the surface ectoderm. The optic vesicle induces the surface ectoderm to form a lens placode, which invaginates and eventually detaches to form the lens vesicle, which will one day become the lens. The surface ectoderm also forms the corneal epithelium, above the area of the lens vesicle[2]. This process begins around the end of the first month of gestation in human, and around day E11-E12 in mouse[2]. Mesenchymal cells surrounding the area of the presumptive retina migrate to form the stroma between the corneal epithelium and lens[2]. Corneal endothelium is derived from neural crest cells and develops around the same time as the stroma[2].

1.3 The Corneal Wound Healing Response

When the cornea is injured, cellular responses are initiated to begin healing the cornea, but some of these responses can compromise its uniquely transparent feature. Several growth factors, including transforming growth factor-beta (TGF-β) and platelet derived growth factor (PDGF) have been shown to be involved in interactions between the corneal epithelium and the stroma during wound healing[8,9,10]. Under normal circumstances, TGF-β and PDGF are produced at low levels in the corneal epithelium, but these growth factors are segregated from the stroma by components of the epithelial basement membrane (EBM), including collagen type IV, laminins, perlecans, and nidogens[11]. If an injury to the cornea disrupts the EBM, TGF-β and PDGF can infiltrate the stroma[8,9,11].

Once TGF-β and PDGF enter the stroma, keratocytes surrounding the injury are stimulated to become myofibroblasts[8,9,11]. Fibroblasts derived from fibrocytes from bone marrow have also been found in the cornea during times of injury[8]. The source of fibroblasts in the cornea can vary greatly[8]. Regardless of origin, fibrocytes and transformed keratocytes develop into mature myofibroblasts as the injury persists[8,9,11]. Fibroblast presence alone reduces the transparency of the stroma, as fibroblasts are less transparent than the normally present keratocyte[13].

Determining the stage of maturity of myofibroblasts in the stroma can aid in determining their potential to reduce transparency, as well as estimating the progression of injury. Maturity of myofibroblasts can be determined through their particular expression of vimentin, alpha-smooth muscle actin (αSMA), and desmin[8]. Vimentin and desmin are known intermediate filament proteins, while αSMA is a protein found in smooth muscle cells as well as in other cell types during wound healing. Inactive keratocytes and immature myofibroblasts first express vimentin while being negative for αSMA and desmin[12]. As the myofibroblast matures, it begins to express both vimentin and αSMA[12]. A fully mature myofibroblast expresses vimentin, αSMA, and desmin, and begins to secrete extracellular matrix components.

The typically present collagen type I is produced in this process, but collagen type I deposited by mature myofibroblasts does not follow the precise organization that stromal collagens naturally follow[12,13]. Additional collagens are produced that are normally present at low levels in the stroma, namely collagen type III[14]. This disorganization of collagen type I and other collagens in the stroma reduces its transparent feature. The decrease in transparency during corneal wound healing caused by the presence of myofibroblasts and deposition of disorganized extracellular matrix is termed corneal haze, corneal scarring, or corneal fibrosis[12,13,15].

Halting the process of corneal fibrosis depends on proper repair and regeneration of damaged epithelial basement membrane. A defective or damaged EBM allows TGF-β signaling to continue and myofibroblasts to fully mature[15]. The EBM can be regenerated within 8-10 days after injury[11]. A hypothesis for prolonged corneal fibrosis postulates that even once the EBM is regenerated, this new basement membrane requires the aid of keratocytes to fully restore components of the EBM[15]. Therefore, if keratocytes are no longer present in the anterior stroma, due to either apoptosis or transformation into myofibroblasts, this new EBM remains defective until keratocytes can enter the area[11,15]. Corneal fibrosis can sometimes take several months to years to completely resolve. Once the EBM is repaired, interleukin-1 alpha (IL-1α) signals myofibroblasts to undergo apoptosis, and transparency is achieved once again[15].

The pro-fibrotic corneal wound healing response has largely been investigated in the context of injury from trauma, surgery, and infection. Surgical procedures such as photorefractive keratectomy (PRK) have been shown to cause corneal fibrosis, evident a few weeks post-procedure[11,16]. In rabbit corneas, myofibroblast development could be seen as soon as two weeks post-PRK, with myofibroblasts fully maturing by four weeks post-PRK[16]. In mouse cornea, presence of α-SMA can be seen four weeks post-PRK[19]. Factors such as irregularity in corneal surface and correction of high myopia have been found to increase the likelihood of developing corneal fibrosis post-PRK[16]. Infection such as microbial keratitis has also been shown to trigger a pro-fibrotic response[11]. This pro-fibrotic response has largely been uninvestigated in other contexts such as genetic disease.

1.4 Aniridia

Aniridia, an ancient Greek term for "without rainbow", is a rare genetic disorder that affects many aspects of the eye's anatomy and physiology[17]. The most striking feature of this disorder is the partial or complete loss of the iris, termed iris hypoplasia[18].

Congenital aniridia is most commonly caused by a mutation in the *PAX6* gene[18,21]. The *PAX6* gene is referred to as a master regulator gene, as it is highly conserved amongst species and has a requirement in normal embryonic development[22,23]. *PAX6* is expressed during development in the eye as well as the brain, pineal gland, pancreas, and other areas[21,22,23,24]. In mouse, homozygous null mutations are lethal during embryogenesis[24]. In human, homozygous null mutations are extremely rare, but lead to anophthalmia and lethal embryonic defects[27]. After development, *PAX6* continues to be expressed in structures of the eye, including the corneal epithelium, iris, and retina[21].

The *PAX6* gene has two main isoforms: the canonical *PAX6* and *PAX6(5a)*[21]. Canonical PAX6 has 14 exons, while PAX6(5a) has an additional exon between exons 5 and 6[25]. Both isoforms have been found to be expressed during development of the eye[25]. *PAX6* contains both a paired domain (PD) and homeodomain (HD)[25]. *PAX6* codes for a transcription factor, which can autoregulate via an upstream ectodermal enhancer (EE) region[25]. Several direct and indirect downstream targets of *PAX6* in human and *Pax6* in mouse have been identified, including transcription factors *Pax2* and *Six3*, crystallin and keratin proteins, cell adhesion molecule *Llcam*, pancreatic hormone *Insulin*, and more.[27] In mouse, downstream targets of *Pax6* shown to be involved in iris and ciliary body development include *Foxc1* and *Bmp4*[26].

Understanding the genetic alterations in aniridia has led to the development of a mouse model of the disease. With a heterozygous null mutation in *Pax6*, mice display microphthalmia, iris hypoplasia, and other physiological abnormalities commonly seen in human aniridia[24]. Mice with *Pax6* deletions leading to a heterozygous null mutation are called Small Eye (*Sey*) due to the microphthalmia phenotype[24].

There are characteristic structural changes seen in aniridic patients. Iris hypoplasia is seen to varying degrees, from partial reduction of iris tissue to complete reduction resulting in an iris stump[18]. Along with iris hypoplasia, aniridia also causes foveal hypoplasia, where the specialized area of the central retina called the fovea is reduced or absent[18]. Hypoplasia of the optic nerve, the culmination of retinal fibers that send signals to the brain, can also occur[18]. Deficiency in the limbal epithelial stem cell niche has been reported[21]. Meibomian gland dysfunction and tear film insufficiency have additionally been reported in aniridia patients[21]. Other structural changes of the eye can include congenital lens opacity, optic nerve coloboma, ptosis, and keratopathy. In the mouse model *Sey*, similar physiological changes are seen, including varying degrees of iris hypoplasia and corneal and lens opacities[24].

In both human and mouse, morphological changes has been shown in the cornea. *In vivo* assessment of central corneal thickness (CCT) by applanation pachymetry has shown an increased CCT in aniridia patients[29]. Anterior segment changes were evaluated histologically in children with congenital aniridia, before the onset of significant aniridia-related complications. A few cases were found to have a thin Bowman's membrane, in some areas replaced by pannus/fibrovascular tissue[31]. Some cases of corneal epithelial atrophy and presence of goblet cells were seen[31].

Histological assessment of *Sey* mice has shown reduction in corneal epithelium and a hypercellular stroma with disorganized lamellar arrangement at postnatal day 14[30] . Furthermore, young *Sey* mice had "interrupted" Bowman's layer in some areas, though this feature is difficult to visualize with histology[30]. Other uncommon abnormalities were seen, such as an epithelial plug with lens fragments present in the cornea[30]. In both human and *Sey* mice, other layers of the cornea, including the endothelium and Descemet's membrane, have not shown any morphological changes.

Since multiple structures of the eye are altered, Aniridic patients experience a myriad of ocular conditions. Without a fully formed iris controlling the amount of light entering the eye, individuals with aniridia experience photophobia[20]. Structural changes to the anterior segment of the eye causes patients to commonly experience increased intraocular pressure, leading to ocular hypertension and glaucoma[18]. Foveal and iris hypoplasia, as well as corneal and lens opacities lead to decreased visual acuity[18]. Due to corneal and lens abnormalities, refractive errors such as myopia and astigmatism are also experienced in aniridic patients[18].

There is currently no cure for aniridia, though there are treatment options available. Dry eye is a common ailment in aniridia patients due to Meibomian gland dysfunction, so typical dry eye treatments are employed such as use of rewetting drops and lubricants[21]. Increased intraocular pressure can be treated with eye drops such as prostaglandin analogs, beta blockers, and Rho kinase inhibitors[32]. Surgical intervention such as trabeculotomy and valve implant have been performed in aniridic patients with a high success rate of managing intraocular pressure[21]. Removal and replacement of the intraocular lens has been used to treat lens opacities[21]. To improve visual acuity, non-surgical measures such as spectacles and contact lenses are used. Surgically, a prosthetic iris implant is a potential treatment to improve visual acuity[33].

1.5 Aniridia-Related Keratopathy

Aniridia-related keratopathy (ARK) is a symptom of aniridia that patients often experience, though not immediately. Although onset of ARK can occur as soon as adolescence, the median age of onset is in patients' early 30's[28]. Previous literature has reported anywhere from 20%-80% of patients exhibit ARK[21,28]. Just as physiological features of aniridia can vary, so can the onset, rate of progression, and severity of ARK[28]. Characteristic changes to the cornea occur in ARK, including conjunctivalization, vascularization, and opacification.

Conjunctivalization refers to the infiltration of conjunctival epithelial cells, or goblet cells, into the cornea. In ARK, conjunctivalization starts in the peripheral cornea, creeping into the central cornea over time[28]. *In vivo* confocal microscopy of aniridic corneas has led to an association between limbal stem cell deficiency(LSCD) and conjunctivalization: in more severe cases of LSCD, more goblet cells were present in the cornea[34]. Therefore, degree of conjunctivalization has been proposed as a tool to determine the degree of LSCD. The mouse model *Sey* has been assessed for conjunctivalization through histology and has likewise shown the presence of goblet cells in the cornea that progress with age[30].

As mentioned previously, the corneal is typically an avascular structure. In human aniridia, presence of fibrovascular tissue, also termed pannus, can be seen in the limbal region before ARK symptoms occur[21,28,31]. Pannus is used to aid in staging of severity of ARK[21,28]. Earlier stages do not display pannus in the cornea, while intermediate stages include pannus in the peripheral cornea[21,28]. Late stage ARK includes pannus in the peripheral and central cornea. Similarly, *Sey* mice show progressive corneal pannus in the anterior stroma, that in some cases obliterates Bowman's membrane[30].

Corneal opacification is an indicator of ARK, and among one of the primary symptoms of aniridia that contributes to vision loss. In human ARK, clouding typically starts in the periphery of the cornea, or starts as an overall haze across the entire cornea[35]. Clouding associated with ARK has been shown to increase with age[35]. Intraocular surgery has also been shown to increase corneal clouding, independent of age[21,35]. Corneal opacification in *Sey* mice has not been thoroughly investigated.

Severity of ARK is staged in humans based on a number of factors: pannus, epithelial damage assessed via fluorescein uptake, opacification, and frequency of corneal ulceration/erosion. Stage 1 is typically characterized by peripheral corneal changes including fluorescein uptake and pannus[21,28]. Stage 1 can also include infrequent but recurring ulceration[21]. Stage 2 involves the same factors as Stage 1, but increased peripheral involvement and corneal erosion[21,28]. Stage 3 includes fluorescein uptake in the central cornea, increased neovascularization, and chronic corneal erosion/ulceration[21,28]. Stage 4 shows abnormal epithelium across the entire cornea with subepithelial opacification. End stage ARK, or Stage 5, shows chronic corneal opacification in the stroma with abnormalities in corneal epithelium[28]. While symptoms of ARK have been assessed histologically in *Sey* mice, clinical evaluation and staging of ARK symptoms in *Sey* has not yet been attempted[30].

Treatment options are available for patients experiencing aniridia-related keratopathy, but the long-term success of these options is limited. As ocular surface integrity is compromised due to tear film insufficiency, Meibomian gland dysfunction, and changes in ocular surface adhesions, lubricants and rewetting drops are used to help maintain a healthy tear film to protect the ocular surface[21]. Several types of surgical intervention have been employed in aniridic patients with variable success. The most successful procedures have been those that involve

enriching or replacing the existing stem cell niche, called limbal stem cell transplantation (LSCT)[28]. One form of LSCT transplants the limbal region from a cadaver cornea around the limbus of the patient's cornea, termed keratolimbal allograft (KLAL)[37]. Another LSCT technique termed living related conjunctival limbal allograft (lr-CLAL) transplants a portion of a living donor's limbus and conjunctiva to the patient[37]. KLAL has been shown to improve the ocular surface and visual acuity in patients with aniridia[37]. However, a majority of patients needed subsequent corneal transplantation, also called penetrating keratoplasty (PK), to diminish corneal scarring and attempt to improve visual acuity, which has a low level of long-term success[28,37]. Patients also require systemic immunosuppression medication for an extended period of time to lessen the chances of graft rejection and improve surgical outcomes[37].

Another surgical treatment method for ARK is the keratoprosthesis (KPro). This method replaces the patient's natural cornea with a prosthetic cornea. A prosthesis eliminates the need for a cadaveric or living related donor. In one study, a majority of patients with ARK experienced retention of the keratoprosthesis and improved visual acuity six months post-operation[38]. However, visual acuity began to decrease in patients over time, and some even experienced prosthesis rejection and worsened visual acuity at time of operation[38]. Furthermore, KPro poses significant risk to the patient that may counteract any gains in visual acuity, including glaucoma and infectious endophthalmitis[38,39]. Use of topical antibiotic medication for the patient's lifetime reduces the risk of vision-threatening infection[39]. Typically, use of KPro is only employed if the prognosis of PK is poor[38,39]. More avenues for treatment options for patients suffering from ARK should be explored, as existing treatment options are not sufficient.

1.6 Hypotheses for Causes of Corneal Clouding in ARK

There are several hypotheses for the cause of the visually detrimental corneal opacification seen in ARK. A widely recognized hypothesis is limbal stem cell deficiency (LSCD). Currently, conjunctivalization and vascularization of the cornea are taken as signs of LSCD in both human and *Sey* mice[21,28,30]. Goblet cells and vascular tissue are less transparent than native corneal tissue. Normally, the limbal epithelial stem cell (LESC) niche segregates these tissues from entering the cornea. Therefore, LSCD is hypothesized to contribute to corneal clouding by allowing the encroachment of goblet cells and vascular tissue as the LESC population degrades. As mentioned previously, *in vivo* studies in human revealed a correlation between altered limbal architecture and conjunctivalization in aniridic patients[34]. However, there are currently no definitive markers for LESC's, so population size of LESC's between $PAX6^{+/+}$ and $PAX6^{+/-}$ cannot be directly compared.

Another hypothesis for corneal clouding in ARK is changes in ocular surface integrity. Studies have shown a reduction in cell adhesion molecules normally present in the corneal epithelium, such as keratin-12 and catenins[30,36]. Fluorescein uptake, an indicator of epithelial cell damage, has been shown to increase in human aniridia[28]. Epithelial cell fragility may allow for corneal scarring in subsequent layers that reduces transparency, as that protective barrier has been compromised or removed. Ocular surface integrity may play a role in corneal clouding, although the correlation of corneal clouding to ocular surface integrity has not been investigated in a mouse model.

Corneal fibrosis as part of the wound healing response could play a role in clouding seen in ARK. Epithelial basement membrane integrity is crucial to preventing activation of keratocytes into myofibroblasts, causing disordered ECM to be deposited[15,16]. Presence of

myofibroblasts and deposition of disordered collagens reduces transparency of the cornea. The epithelial basement membrane has been cited as altered or partially obliterated in aniridia, so the barrier preventing a pro-fibrotic response from occurring could be compromised. Furthermore, the corneal epithelium has been shown to be reduced in human aniridia and the *Sey* mouse model, which may allow the EBM to be damaged more frequently[29,30]. Reduced transparency may be due to a chronic wound healing response in the cornea. In mouse, the pro-fibrotic response has been shown to occur after surgery, trauma, and infection, but has not yet been investigated in the *Sey* model.

The current study aims to investigate a few of the hypotheses of contributions to corneal clouding in ARK. Specifically, the hypotheses of ocular surface integrity, conjunctivalization, and the pro-fibrotic response will be investigated. Using the *Sey* model, mice will be investigated at time points that capture mild ARK symptoms (17-19 weeks old) and severe ARK symptoms (40+ weeks old). Clinical evaluation will be performed, and ocular surface integrity will be assessed through fluorescein uptake. Histological evaluation will be used to visualize morphological changes in the cornea as well as goblet cell infiltration as a measure of conjunctivalization. Using immunofluorescence, the pro-fibrotic response will be investigated for the first time in *Sey* mice, using a myofibroblast marker (α-SMA) and a corneal wound healing marker (collagen type III).

CHAPTER 2

INVESTIGATING THE CAUSES OF CORNEAL CLOUDING IN ANIRIDIA-RELATED KERATOPATHY

2.1 Materials and Methods

Animal Use and Maintenance

All animal procedures were conducted in accordance with the guidelines and approval of the University of Georgia Institutional Animal Care and Use Committee (IACUC). *Pax6*$^{+/-}$ (*Sey*^{neu}) and *Pax6*$^{+/+}$ (wild-type) littermates were generated from *Pax6*$^{+/-}$ females crossed with *Pax6*$^{+/+}$ males. Mice were bred on an albino CD-1 background and maintained at the Coverdell Rodent Vivarium at the University of Georgia. Mice were weaned at 21-25 days postnatal. Tail clips were collected at time of weaning. Ear punches were performed at time of weaning as a means of identification. Littermates of the same sex were housed together after weaning. Mice were aged to two time points: 17-19 weeks old (during onset of mild ARK symptoms) and 40+ weeks old (severe ARK symptoms).

Genotyping

Mouse breeding pairs and progeny were assessed phenotypically by eye size and confirmed genotypically by polymerase chain reaction (PCR). Genomic DNA was extracted from tail clips taken at time of weaning. For detection of *Pax6*, forward primer (5' GGA ATT CCT GAG GAA CCA GAG AAG ACA GGC 3') and reverse primer (5' GCA TAG GCA GGT TGT TTG CC 3') were used. A 20µl PCR volume was made for each sample, containing 2µl

genomic DNA, 2µl 10X PCR Buffer Taq (contains $MgCl_2$), 0.5µl of 10mM dNTP Mix, 0.2µl of 20µM Forward Primer, 0.2µl of 20µM Reverse Primer, 0.2µl Dream Taq DNA Polymerase, and 14.9µl diH_2O. Thermal cycler settings were as follows: one cycle of 2 min at 95ºC, 34 cycles of 1 min at 95ºC, 30s at 60ºC, and 30s at 72ºC, one cycle of 5 min at 72ºC. For detection of *Pax6* mutation, restriction digest was performed with 15µl of PCR product, 2µl of NE Buffer, and 1µl of Hind II/Hinc II enzyme per sample incubated at 37ºC for at least one hour. Remaining PCR product was stored at 4ºC. Digested and un-digested PCR product were separated on a 2% agarose gel with 4 µl SYBR Safe added to gel. Wild-type *Pax6* generated a 318 bp fragment, while mutant *Pax6* generated 250 bp and 68 bp fragments.

Clinical Evaluation

For more details on clinical evaluation, including detailed fluorescein uptake protocol, clinical exam sheet template, and scoring rubrics, see Appendix. At specified time points, mice were euthanized with CO_2. Cervical dislocation was used as a secondary measure of euthanasia. During clinical evaluation, the ocular surface was kept moisturized with sterile eye irrigating solution (Bausch + Lomb Advanced Eye Relief® Eye Wash). Eyes were scored for presence of iris, corneal clarity, lens clarity, lens placement, and ocular surface integrity. Fluorescein uptake was used to assess ocular surface integrity; approximately 100µl of fluorescein solution was applied to the ocular surface for 60s, then thoroughly rinsed with eye irrigating solution. Images were taken pre- and post-fluorescein uptake with a stereo microscope (SteREO Discovery V.12, Carl Zeiss Micrscopy, LLC) with FITC480 fluorescence filter (X-Cite® 120Q Fluorescence Lamp, Excelitas Technologies).

Histology

After clinical evaluation, the right eye of each mouse was fixed in 4% paraformaldehyde in PBS at 4ºC overnight. Eyes were dehydrated in ethanol, rinsed in pure xylene, then embedded in paraffin wax. 7μm serial sections were cut in a sagittal orientation through the whole eye. Sections closest to the central region of the cornea were used for histological staining. One slide from each eye was stained with hematoxylin and eosin. Another slide from each eye underwent PAS staining to detect goblet cells: slides were treated with 0.55% periodic acid for 5 min, then stained with Schiff reagent for 15 min, then run under warm water until color of sections developed from a light pink to a dark pink/purple. Images of histology were obtained on a Keyence microscope (BZ-X800 All-in-one Fluorescence Microscope, Keyence Corporation of America).

Analysis of PAS Staining

After PAS staining, images from five sections as close to the central cornea as possible were taken and stitched together to form five full images of the cornea from periphery to center (BZ-X800 All-in-one Fluorescence Microscope, Keyence Corporation of America). PAS-stained cells were counted per image, then counts for the five images were averaged for each sample. Averages from each sample were then grouped by time point (17-19 weeks old and 40+ weeks old) and genotype (wild-type and *Sey*^{neu}) and total averages were taken for each time point and genotype. Statistical analysis was performed on these averages using SPSS (IBM Corp. Released 2020. IBM SPSS Statistics for Windows, Version 27.0. Armonk, NY: IBM Corp.).

Immunofluoresence

After clinical evaluation, the left eye of each mouse was fixed in 4% paraformaldehyde in PBS at 4°C overnight. Eyes were processed in 15% sucrose in PBS at 4°C overnight, then 30% sucrose in PBS at 4°C overnight. Eyes were rinsed in O.C.T. medium then embedded in O.C.T. at -80°C overnight (Tissue-Plus™ O.C.T. Compound, PANTek Technologies LLC). Sagittal sections of 7μm were cut through the whole eye. Immunofluorescent evaluation was used to detect a pro-fibrotic response, using α-SMA as a myofibroblast marker, and Collagen type III as an indicator of wound healing and presence of mature myofibroblasts. Sections were washed in 1XPBS then blocked in 1XPBS containing 0.3% Triton X-100, 0.2% Bovine Serum Albumin (BSA), and 5% goat serum for one hour at room temperature. Sections were incubated in a 1:1000 dilution of either α-SMA rabbit polyclonal primary antibody (ABclonal) or Collagen type III rabbit polyclonal primary antibody (ABclonal) for 16 hours at 4°C. Sections were then rinsed in 1XPBS with 0.3% Triton X-100 (PBS-T) and incubated in a 1:200 dilution of donkey anti-rabbit IgG Alexa Fluor 568 secondary antibody (Invitrogen) for two hours at room temperature. Sections were again rinsed in PBS-T, then incubated in 300nM 4',6-diamidino-2-phenylindole (DAPI) for 10 min at room temperature to achieve nuclear staining. Sections were mounted in 70% glycerol, then covered with a glass coverslip and sealed on the edges of the coverslip with clear nail polish. Immunofluorescent images were obtained on a Keyence microscope in brightfield, red, and blue channels (BZ-X800 All-in-one Fluorescence Microscope, Keyence Corporation of America). Images in each channel were merges using Keyence BZ-X Analyzer software (BZ-X800 All-in-one Fluorescence Microscope, Keyence Corporation of America).

2.2 Results

Clinical Evaluation of 17-19 Week Old Mice

At 17-19 weeks old, wild-type (*Pax6*$^{+/+}$) mice displayed excellent corneal clarity, lens clarity, and lens placement (n=10) (Figure 1A). Only one eye had an instance of decreased corneal clarity resulting in some loss of iris detail (not shown). In *Sey* (*Pax6*$^{+/-}$), all eyes had decreased corneal clarity (n=6). One eye had severe corneal clouding (Figure 1D). Lens clarity and lens placement were undetermined due to corneal haze obstruction. Ocular surface integrity was assessed via fluorescein uptake. In wild-type, zero to low fluorescein uptake was found in a majority of eyes (n=10)(Figure 1C). One wild-type eye had increased fluorescein uptake (not shown). In *Sey*, fluorescein uptake was found in all eyes (n=6)(Figure 1F). Four eyes had increased fluorescein uptake, with two eyes displaying mild fluorescein uptake while the other two had more severe fluorescein uptake. Clinical findings in 17-19 week old mice are summarized in Table 1.

Clinical Evaluation of 40+ Week Old Mice

At 40+ weeks old, a majority of wild-type (*Pax6*$^{+/+}$) mice had excellent corneal clarity (n=6)(Figure 2A). Two eyes showed slightly decreased corneal clarity resulting in some loss of iris detail, similar to what was seen in one eye at the 17-19 week old time point (not shown). Lens placement and lens clarity were excellent in all wild-type eyes. Assessment of ocular surface integrity showed an increase in punctate uptake as compared to earlier time points (n=6)(Figure 2C). Half of 40+ week old wild-type eyes showed low fluorescein uptake, and one

eye showed mild punctate uptake (not shown). In *Sey* (*Pax6*$^{+/-}$), corneal clarity further decreased as compared to the earlier time point (n=6)(Figure 2D). Half of these eyes showed mild corneal clouding; additionally, two eyes had severe corneal clouding (not shown). Lens clarity and lens placement was undetermined for all *Sey* mice at this time point. Ocular surface integrity also decreased as compared to 17-19 week old *Sey* (n=6). Half of these eyes had severe fluorescein uptake (Figure 2F). Two eyes had mild fluorescein uptake (not shown). Clinical findings in 40+ week old mice are summarized in Table 2.

Histological Evaluation of 17-19 Week Old Mice

After clinical evaluation, the right eye of each animal was processed for histology (Figure 3). For hematoxylin and eosin staining, wild-type (*Pax6*$^{+/+}$) mice had normal morphological findings (n=5) (Figure 3A). In *Sey* (*Pax6*$^{+/-}$), hematoxylin and eosin staining confirmed findings of corneal epithelial thinning and stromal hypercellularization seen in previous literature (n=3)(Figure 3B, 3C). The endothelium appeared normal. The EBM and Descemet's membrane could not be visualized with histology. For PAS staining of goblet cells, wild-type (*Pax6*$^{+/+}$) had one section with one goblet cell present, but the remaining sections and samples were completely devoid of goblet cells (n=5)(Figure 5A). *Sey* (*Pax6*$^{+/-}$) had goblet cells present in all samples (n=3)(Figure 5B). Averages of PAS staining are outlined in Table 3

Histological Evaluation of 40+ Week Old Mice

After clinical evaluation, the right eye of each animal was processed for histology. Hematoxylin and eosin staining showed normal morphology in wild-type (*Pax6*$^{+/+}$) corneas (n=3)(Figure 4A). *Sey* (*Pax6*$^{+/-}$) continued to display a reduction in epithelium and hypercellular stroma similar to the 17-19 week old time point (n=3)(Figure 4B). At this older time point, more epithelium irregularities were seen; one eye showed an area of epithelial thickening where the stroma had been diminished (Figure 4C). Another eye had a mass of epithelial cells congregating in the peripheral cornea (not shown). *Sey* mice also displayed pockets of fibrovascular tissue in the anterior stroma (Figure 4D). PAS staining again was only seen in one section of one eye in wild-type corneas (n=3). The rest of the sections observed were clear of goblet cells (Figure 6A). Goblet cells were present in *Sey* corneas at this time point (Figure 6B). Although there was an increase in goblet cells in 40+ week old *Sey* corneas as compared to wild-type at the same time point, conjunctivalization decreased as compared to *Sey* mice in the earlier time point. Averages of PAS staining are outlined in Table 4.

Statistical Analysis of PAS Staining

Two-way Analysis of Variance (ANOVA) was performed on average PAS-stained cells for each sample: 17-19 week old wild-type (M=0.04, SD=0.09), 17-19 week old *Sey*^{neu} (M=3.00, SD=1.91), 40+ week old wild-type (M=0.13, SD=0.23), and 40+ week old *Sey*^{neu}(M=0.87, SD=1.33). Average number of PAS-stained cells present in the cornea differed between wild-

type and *Sey*^{neu} mice (df=1, F=10.367, p<0.01)(Figure 7). Average PAS-stained cells did not differ between 17-19 week old and 40+ week old mice (df=1, F=3.163, p=0.106)(Figure 7). Descriptive statistics and analysis are summarized in Table 5.

Immunofluorescent Evaluation of 17-19 Week Old Mice

After clinical evaluation, the left eye of each animal was processed for immunofluorescence, using α-SMA and collagen type III as markers of myofibroblasts and the pro-fibrotic wound healing response. In the mouse eye, α-SMA is normally expressed in the iris and ciliary body (Figure 8). In wild-type (*Pax6*$^{+/+}$) corneas, α-SMA expression was seen infrequently in the epithelium (n=5)(Figure 9). α-SMA expression was not seen in any other corneal layer. Collagen type III was expressed in the epithelium of a majority of wild-type corneas, but not in any other layer (Figure 10). In *Sey* (*Pax6*$^{+/-}$) corneas, α-SMA expression was seen in all samples in the epithelium and endothelium (n=3)(Figure 11). A majority of corneas also had α-SMA expression in the stroma, particularly the anterior portion of the stroma (Figure 11). Collagen type III was expressed in low levels in the epithelium of all *Sey* corneas (Figure 12). One eye had collagen type III expression in the stroma, while no *Sey* corneas had endothelial expression (Figure 12). Results of immunofluorescent evaluation for 17-19 weeks old samples are found in Table 6. α-SMA and collagen type III expression for each genotype and time point are summarized in Table 8 and 9, respectively.

Immunofluorescent Evaluation of 40+ Week Old Mice

After clinical evaluation, the left eye of each animal was processed for immunofluorescence, using α-SMA and collagen type III as markers of myofibroblasts and the pro-fibrotic wound healing response. In wild-type (*Pax6*$^{+/+}$), α-SMA expression was found in all corneas in the epithelium (n=3)(Figure 13). α-SMA expression was also found in one cornea in the stroma (not shown). The endothelium had no α-SMA expression in any sample observed. Wild-type corneas had collagen type III expression in low levels in the epithelium of all samples (Figure 14). One eye had collagen type III expression in the stroma, and another eye had expression in the endothelium (not shown). All other corneal layers in other samples did not show collagen type III expression. In *Sey* (*Pax6*$^{+/-}$), α-SMA expression was found in the epithelium and stroma of all samples (n=3)(Figure 15). One eye had endothelial expression (not shown). Collagen type III expression was found in a similar pattern in Sey, with all corneas showing expression in the epithelium and stroma and only one cornea showing expression in the endothelium (Figure 16). Results of immunofluorescent evaluation for 40+ week old samples are found in Table 7. α-SMA and collagen type III expression for each genotype and time point are summarized in Table 8 and 9, respectively.

Genotype	Sex	Age at Evaluation	CC		LC		LP		OSI	
			OD	OS	OD	OS	OD	OS	OD	OS
CD-1	F	19 weeks	0	0	0	0	0	0	1	2
CD-1	F	19 weeks	0	0	0	0	0	0	0	1
CD-1	F	19 weeks	0	0	0	0	0	0	0	1
CD-1	F	19 weeks	0	1	0	0	0	0	1	1
CD-1	M	17 weeks	0	0	0	0	0	0	0	1
Sey^{neu}	F	19 weeks	1	2	ND	ND	ND	ND	2	1
Sey^{neu}	M	17 weeks	2	1	ND	ND	ND	ND	3	3
Sey^{neu}	M	17 weeks	1	3	ND	ND	ND	ND	1	2

Table 1: Clinical evaluation of 17-19 week old mice. OD=right eye, OS= left eye, ND=unable to determine, CC=corneal clarity, LC=lens clarity, LP=lens placement, OSI=ocular surface integrity. Score of 0=excellent, 3=poor. For more details, see Scoring Rubrics in Appendix.

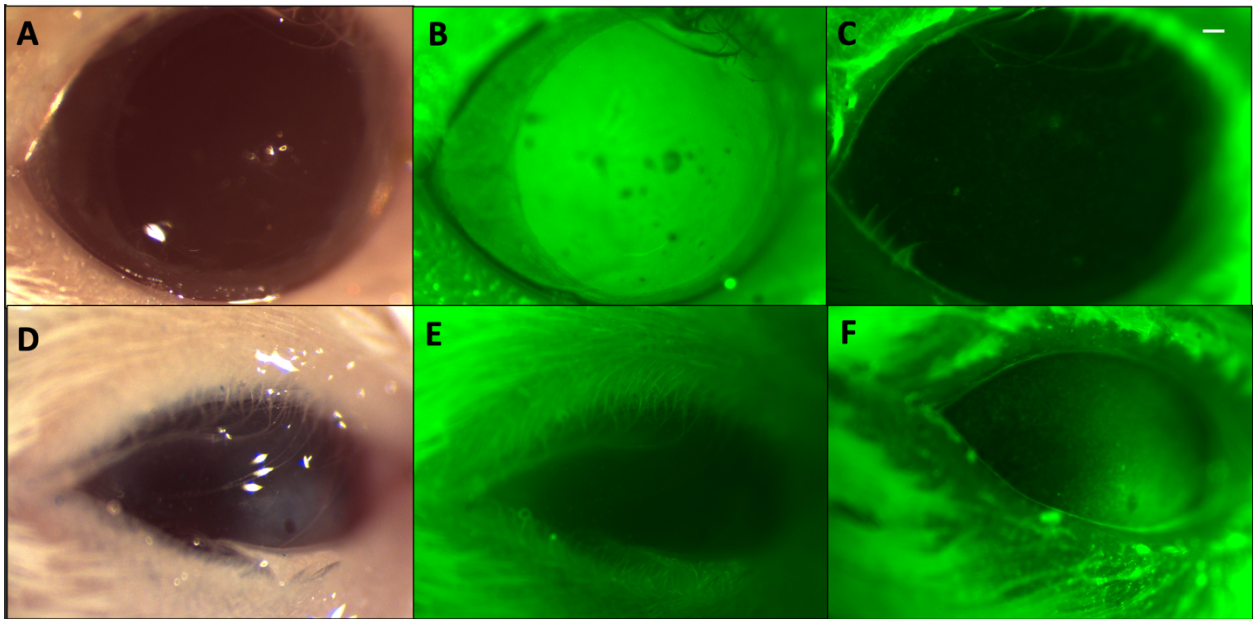

Figure 1: Clinical Evaluation of 17-19 Week Old Mice. (A) 40X image of wild-type eye in brightfield. Cornea and lens are clear and iris detail is clearly visible. (B) 40X image of wild-type eye in FITC 480 filter pre-fluorescein uptake. (C) 40X image of wild-type eye in FITC 480 filter post-fluorescein uptake. A few punctate areas of uptake are seen, but the ocular surface is generally devoid of fluorescein uptake. (D) 40X image of *Sey*^{neu} eye in brightfield. Area of heavy clouding in inferior nasal region, with overall haze. (E) 40X image of *Sey*^{neu} in FITC 480 filter pre-fluorescein uptake. (F) 40X image of *Sey*^{neu} in FITC480 filter post-fluorescein uptake. Large area of fluorescein uptake seen in inferior nasal region, coinciding with region of corneal opacity. Scale bar = 20 μm.

Genotype	Sex	Age at Evaluation	CC		LC		LP		OSI	
			OD	OS	OD	OS	OD	OS	OD	OS
CD-1	F	50 weeks	0	0	0	1	0	0	0	1
CD-1	F	50 weeks	1	0	0	0	0	0	1	1
CD-1	M	43 weeks	0	1	0	0	0	0	0	2
Sey^{neu}	F	50 weeks	2	3	ND	ND	ND	ND	2	3
Sey^{neu}	M	43 weeks	3	2	ND	ND	ND	ND	3	3
Sey^{neu}	M	43 weeks	1	2	ND	ND	ND	ND	1	2

Table 2: Clinical evaluation of 40+ week old mice. OD= right eye, OS= left eye, ND=unable to determine, CC=corneal clarity, LC=lens clarity, LP=lens placement, OSI=ocular surface integrity. Score of 0=excellent, 3=poor. For more details, see Scoring Rubrics in Appendix

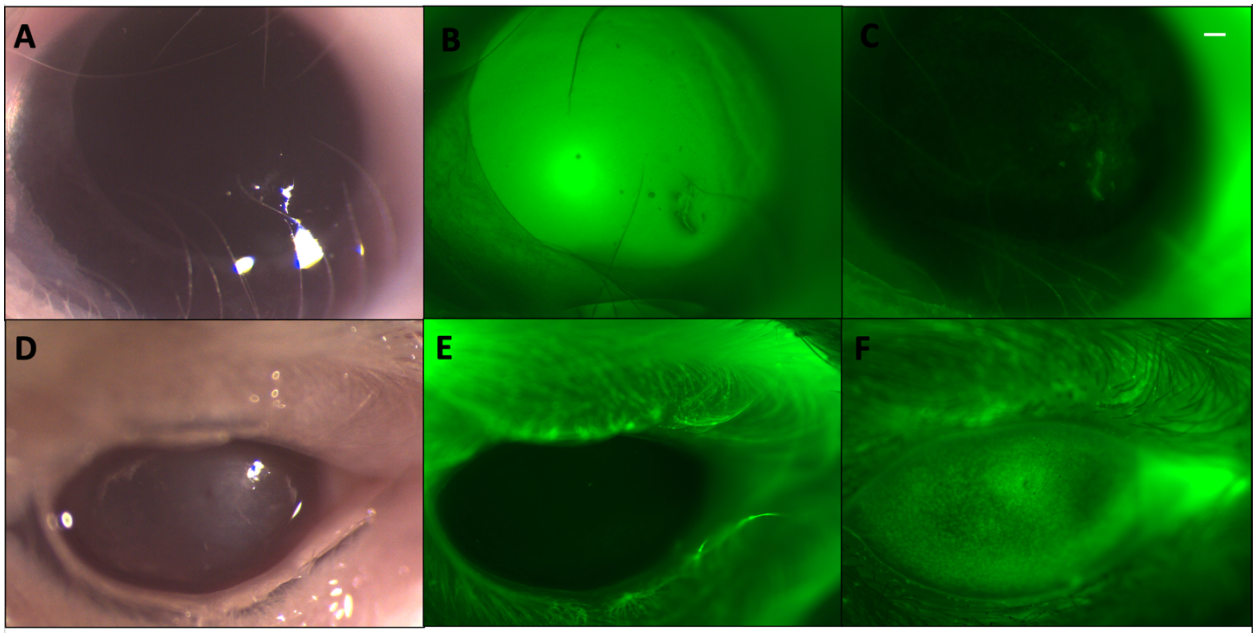

Figure 2: Clinical Evaluation of 40+ Week Old Mice. (A) 40X image of wild-type mouse eye in brightfield. Cornea and lens are clear, with iris detail visible. (B) 40X image of wild-type mouse eye in FITC 480 filter pre-fluorescein uptake. (C) 40X image of wild-type mouse eye in FITC 480 filter post-fluorescein uptake. An area of fluorescein uptake can be seen in the inferior region resulting from possible acute injury, with a few small areas of uptake around the injury. The rest of the ocular surface is free of fluorescein uptake. (D) 40X image of *Sey*^{neu} eye in brightfield. Severe corneal clouding can be seen across the ocular surface, obstructing visualization of more posterior structures. (E) 40X image of *Sey*^{neu} eye in FITC 480 filter pre-fluorescein uptake. (F) 40X image of *Sey*^{neu} eye in FITC 480 filter post-fluorescein uptake. Fluorescein uptake seen across the ocular surface, with increased uptake in the superior central region. Scale bar = 20 μm.

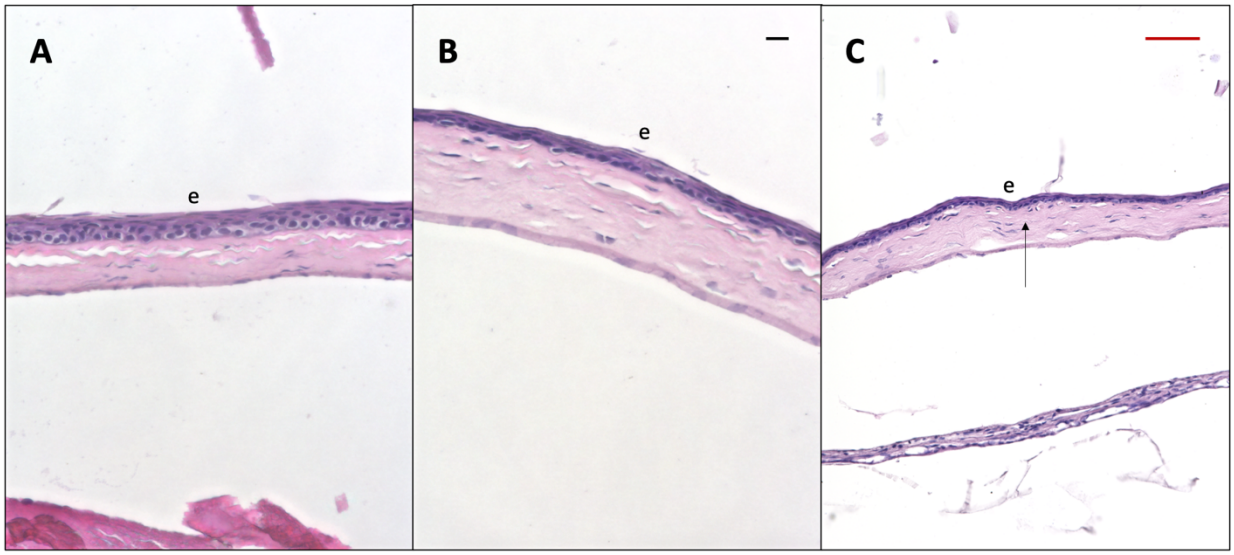

Figure 3: Hematoxylin and eosin staining of 17-19 week old mouse corneas. (A) 40X image of wild-type cornea. Corneal epithelium is 5-7 cell layers thick. (B) 40X image of *Sey*^{neu} cornea. Epithelium has been reduced, and thickening of the stroma is seen. (C) 40X image of *Sey*^{neu} cornea. Corneal epithelium is reduced to a 1-2 cell layer thickness, and thickening with hypercellularization of the anterior stroma is seen (black arrow). Epithelium=e. Black scale bar = 20 μm, red scale bar = 100 μm.

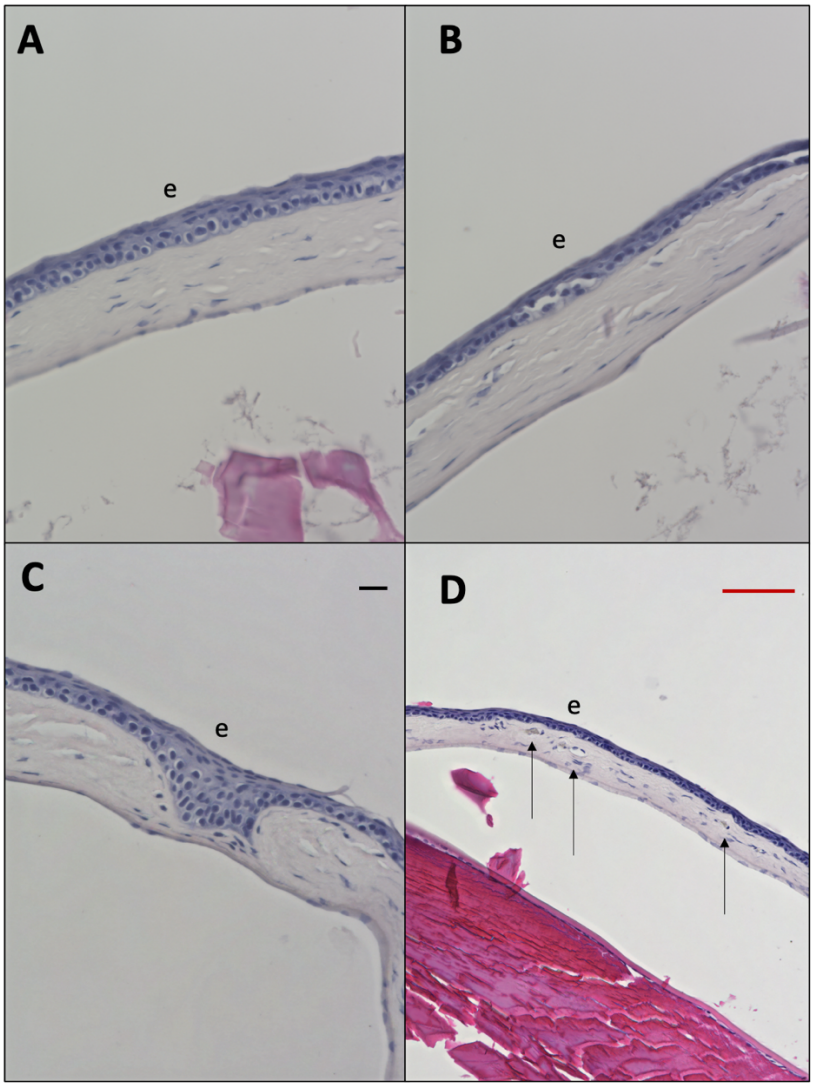

Figure 4: hematoxylin and eosin staining of 40+ week old mouse corneas. (A) 40X image of wild-type cornea, displaying normal epithelial stratification and stromal organization. (B) 40X image of *Sey*^{neu} cornea displaying reduced epithelium. (C) 40X image of *Sey*^{neu} cornea with an epithelial plug replacing the stroma. (D) 20X image of *Sey*^{neu} cornea with fibrovascular tissue infiltrating the stroma (black arrows). Epithelium=e. Black scale bar = 20 μm, red scale bar = 100 μm.

Genotype	Section 1	Section 2	Section 3	Section 4	Section 5	Average PAS
CD-1	0	0	0	0	0	0
CD-1	0	0	0	0	0	0
CD-1	0	1	0	0	0	0.2
CD-1	0	0	0	0	0	0
CD-1	0	0	0	0	0	0
Sey^{neu}	8	7	4	2	4	5.0
Sey^{neu}	4	0	0	1	1	1.2
Sey^{neu}	6	2	2	2	2	2.8

Table 3: Average PAS-stained cells in 17-19 week old wild-type and *Sey* corneas. Five sections of whole cornea for each sample were observed for presence of PAS-stained cells. Scores from these sections were averaged for each sample.

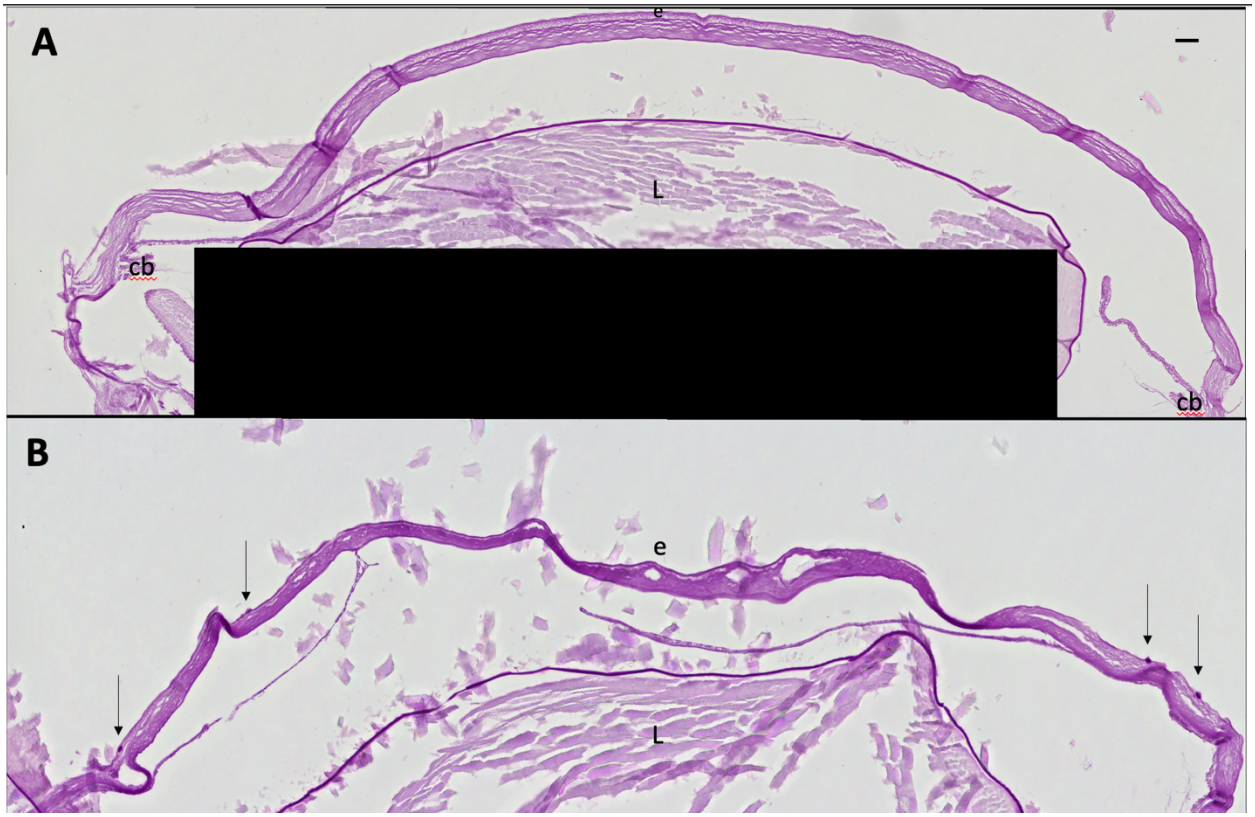

Figure 5: PAS Staining of 17-19 week old mouse corneas. (A) composite image of a cross-section of wild-type cornea, devoid of PAS-stained cells. (B) composite image of a cross-section of *Sey*^{neu} cornea, with PAS-stained cells present in the peripheral cornea (black arrows). Epithelium=e, lens=L, ciliary body=cb. Scale bar = 100 µm.

Genotype	Section 1	Section 2	Section 3	Section 4	Section 5	Average PAS
CD-1	0	0	0	0	0	0
CD-1	0	0	0	0	2	0.4
CD-1	0	0	0	0	0	0
Sey^{neu}	0	0	0	0	1	0.2
Sey^{neu}	7	0	0	0	5	2.4
Sey^{neu}	0	0	0	0	0	0

Table 4: Average PAS-stained cells in 40+ week old wild-type and *Sey* corneas. Five sections of whole cornea for each sample were observed for presence of PAS-stained cells. Scores from these sections were averaged for each sample.

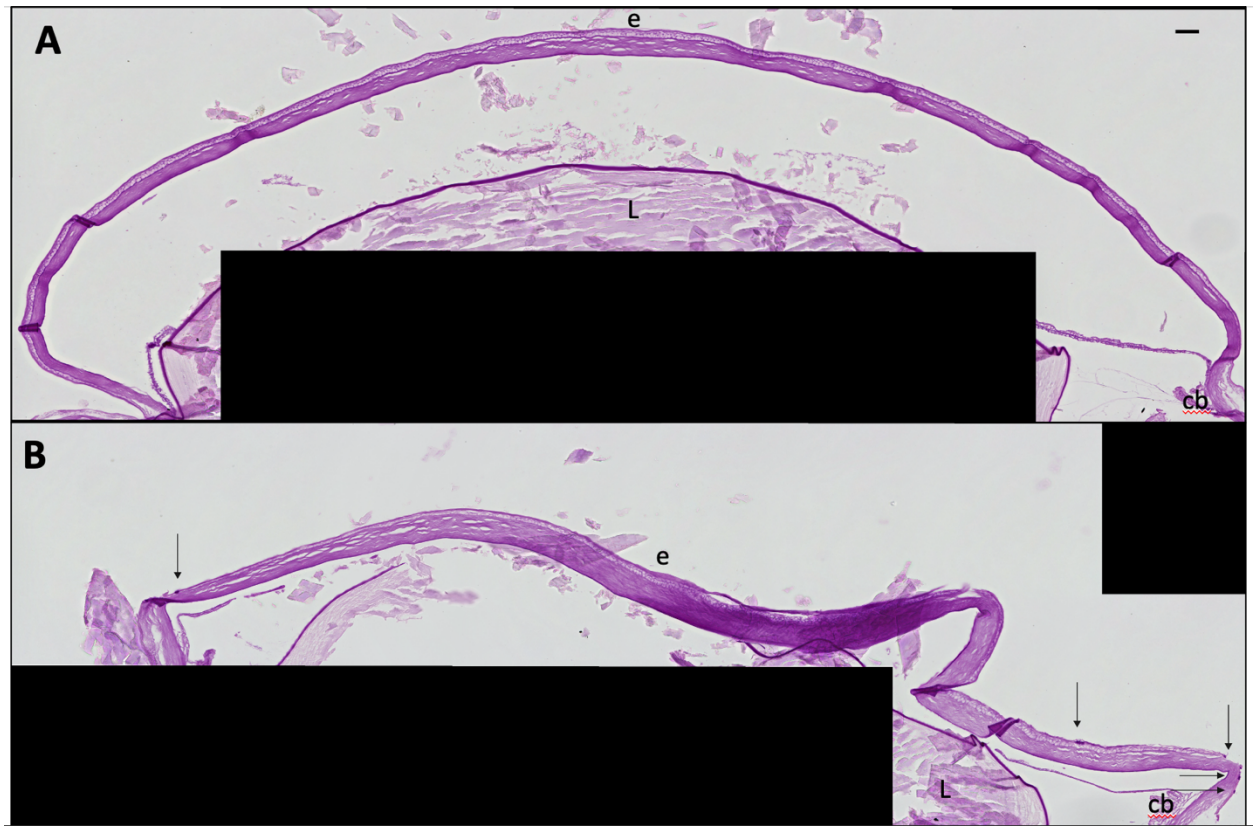

Figure 6: PAS Staining of 40+ week old mouse corneas. (A) composite image of a cross-section of wild-type cornea, devoid of PAS-stained cells. (B) composite image of a cross-section of *Sey*^{neu} cornea, with PAS-stained cells present in the peripheral cornea (black arrows). Epithelium=e, lens=L, ciliary body=cb. Scale bar = 100 µm.

Source	Type III Sum of Squares	df	Mean Square	F	Sig.	Partial Eta Squared
Corrected Model	18.683[a]	3	6.228	5.679	0.016	0.630
Intercept	13.601	1	13.601	12.404	0.006	0.554
Age	3.468	1	3.468	3.163	0.106	0.240
Genotype	11.367	1	11.367	10.367	0.009	0.509
Age * Genotype	4.132	1	4.132	3.768	0.081	0.274
Error	10.965	10	1.097			
Total	40.280	14				
Corrected Total	29.649	13				

a. R Squared = .630 (Adjusted R Squared = .519)

Table 5: Tests of between-subjects effects of age (17-19 weeks and 40+ weeks) and genotype (wild-type and *Sey*^{neu}) on average number of PAS-stained cells. Degrees of freedom=df, F-value=F, significance/p-value=Sig.

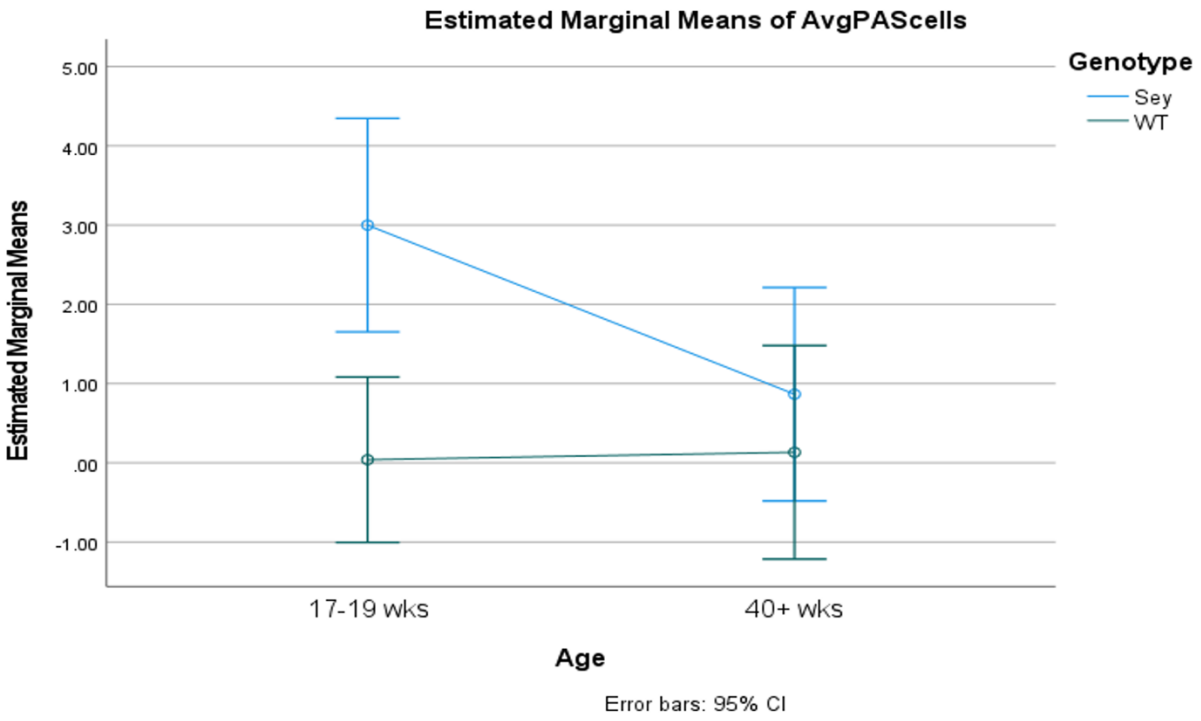

Figure 7: Average number of PAS-stained cells by age and genotype. The blue line represents *Sey*^{neu} (*Pax6*$^{+/+}$) samples. The green line represents wild-type (*Pax6*$^{+/-}$) samples. The x-axis represents each time point (17-19 weeks old and 40+ weeks old). The y-axis represents average number of PAS cells per group. Error bars represent a 95% confidence interval. Average number of PAS cells had a statistically significant difference between *Sey*^{neu} and wild-type at 17-19 weeks old. At the 40+ week old time point, no significant difference was found between average number of PAS cells in *Sey*^{neu} versus wild-type.

Genotype	Alpha-Smooth Muscle Actin			Collagen Type III		
	Epi	**Stroma**	**Endo**	**Epi**	**Stroma**	**Endo**
CD-1	1/3	0/3	0/3	1/1*	0/1*	0/1*
CD-1	0/3	0/3	0/3	2/3	0/3	0/3
CD-1	0/3	0/3	0/3	1/3	0/3	0/3
CD-1	0/3	0/3	0/3	1/3	0/3	0/3
CD-1	2/3	0/3	0/3	0/3	0/3	0/3
Sey^{neu}	3/3	2/3	3/3	2/3	0/3	0/3
Sey^{neu}	3/3	3/3	0/3	3/3	3/3	0/3
Sey^{neu}	0/3	3/3	3/3	1/3	0/3	0/3

Table 6: Expression of α-smooth muscle actin and collagen type III in 17-19 week old wild-type and *Sey*^{neu} mouse corneas. Three sections per sample for each treatment were observed for expression in each layer of the cornea. Epithelium=Epi, endothelium=Endo. *Due to errors in tissue processing, only one sample for this particular treatment for this sample could be included in our study.

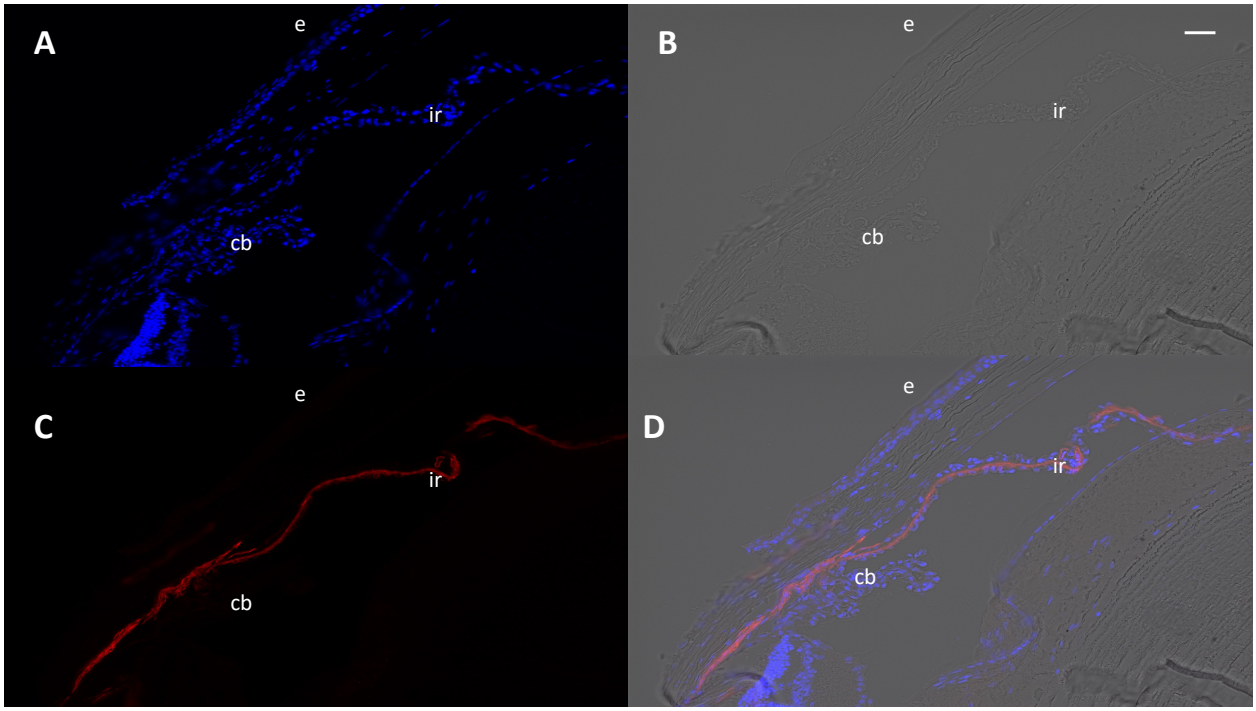

Figure 8: Presence of α-smooth muscle actin in the iris and ciliary body of 17-19 week old wild-type mouse. (A) 40X image in DAPI channel showing nuclear staining. (B) 40X image in brightfield channel. (C) 40X image in red channel showing α-smooth muscle actin expression. (D) 40X merged image of DAPI, brightfield, and red channels. Epithelium=e, ciliary body=cb, iris=ir. Scale bar = 20 μm.

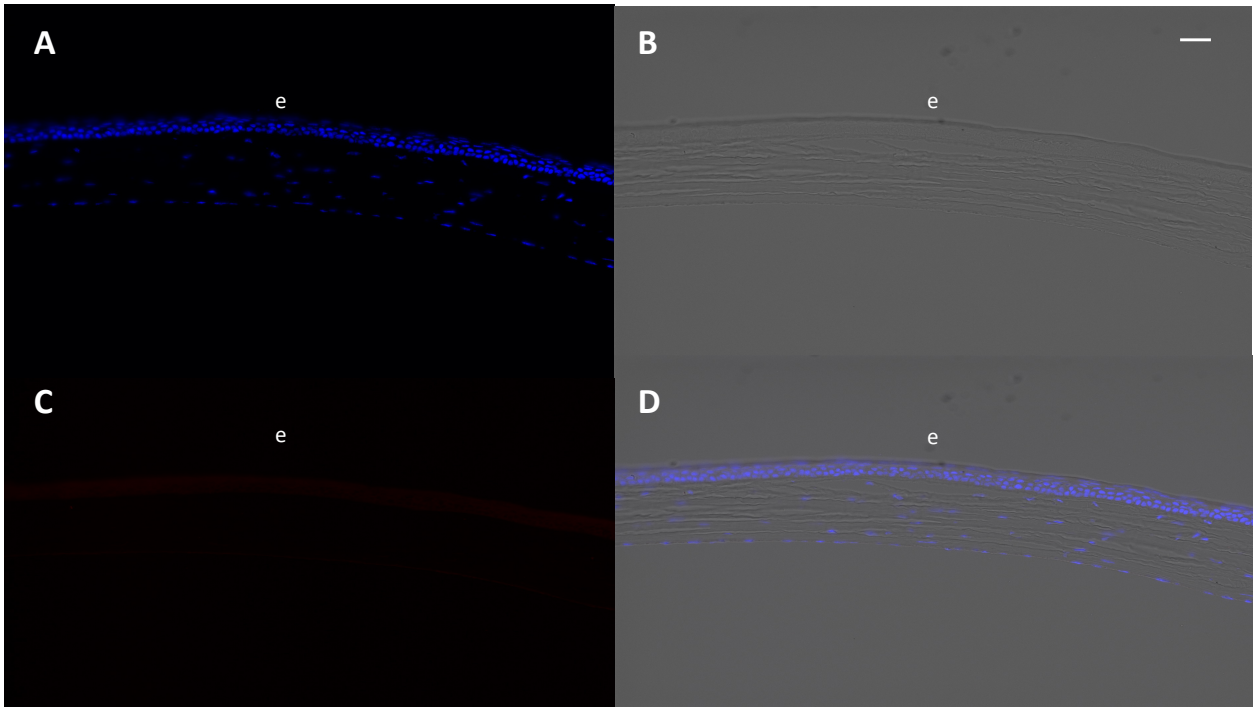

Figure 9: Presence of α-smooth muscle actin in the central cornea of 17-19 week old wild-type mouse. (A) 40X image in DAPI channel showing nuclear staining. (B) 40X image in brightfield channel. (C) 40X image in red channel showing α-smooth muscle actin expression. (D) 40X merged image of DAPI, brightfield, and red channels. Epithelium=e. Scale bar = 20 μm.

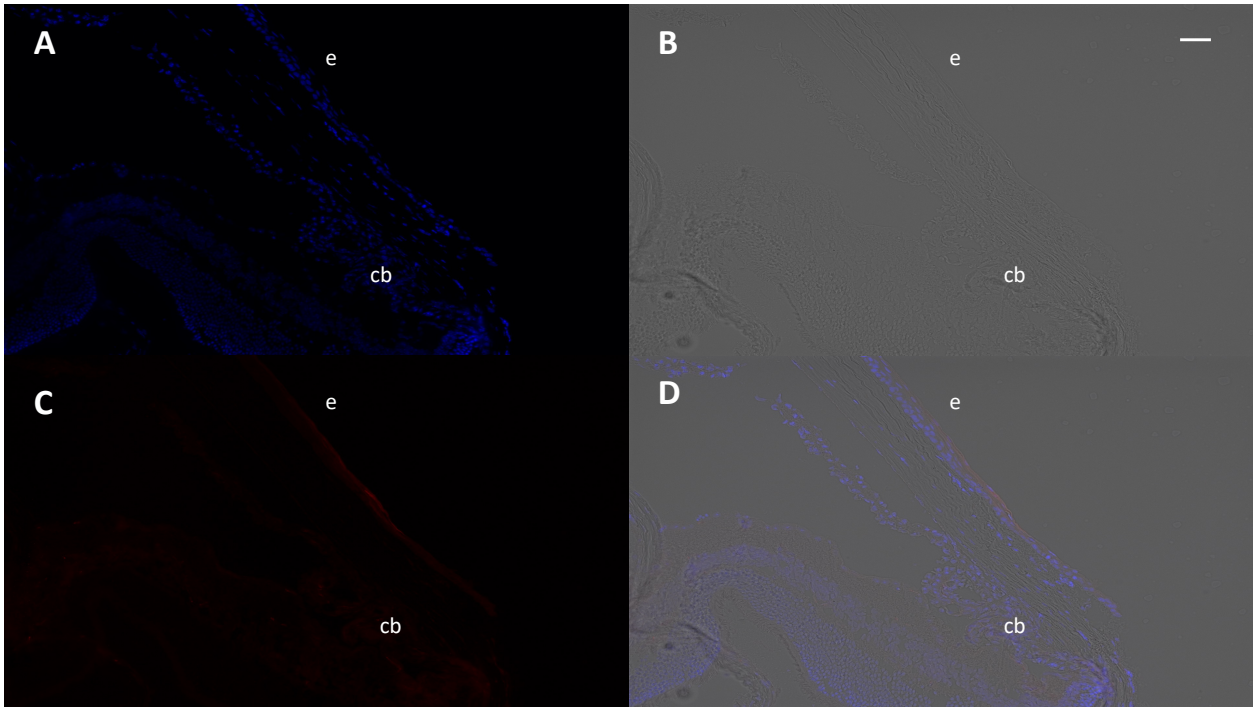

Figure 10: Presence of collagen type III in the cornea of 17-19 week old wild-type mouse. (A) 40X image in DAPI channel showing nuclear staining. (B) 40X image in brightfield channel. (C) 40X image in red channel showing collagen type III expression. (D) 40X merged image of DAPI, brightfield, and red channels. Epithelium=e, ciliary body=cb. Scale bar = 20 μm.

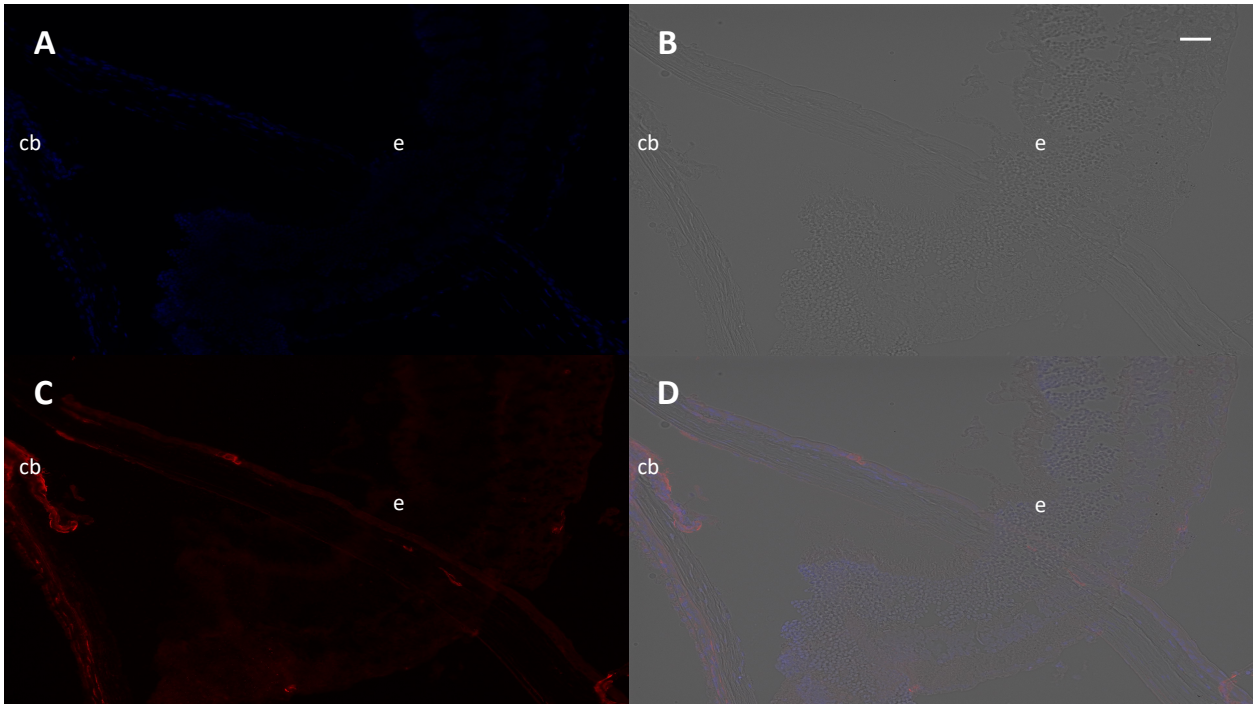

Figure 11: Presence of α-smooth muscle actin in the cornea of 17-19 week old *Sey*^{neu} mouse. (A) 40X image in DAPI channel showing nuclear staining. (B) 40X image in brightfield channel. (C) 40X image in red channel showing α-smooth muscle actin expression. (D) 40X merged image of DAPI, brightfield, and red channels. Epithelium=e, ciliary body=cb. Scale bar = 20 μm.

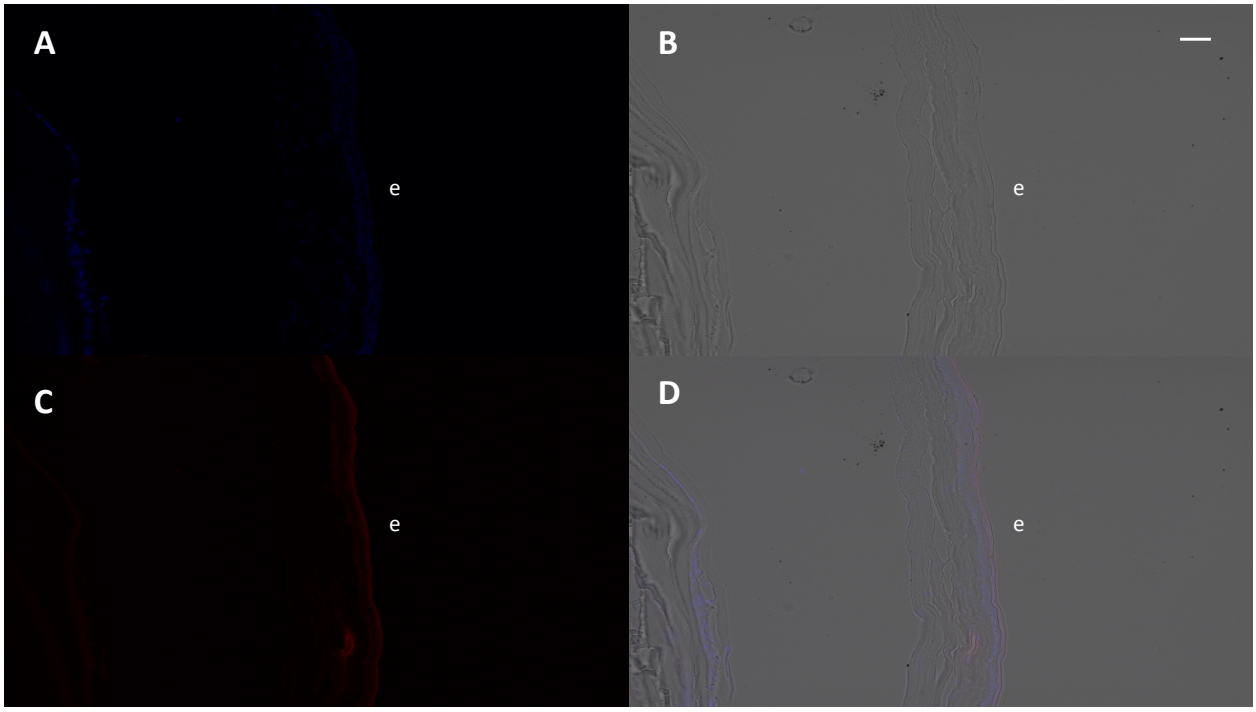

Figure 12: Presence of collagen type III in the cornea of 17-19 week old *Sey*^{neu} mouse. (A) 40X image in DAPI channel showing nuclear staining. (B) 40X image in brightfield channel. (C) 40X image in red channel showing collagen type III expression. (D) 40X merged image of DAPI, brightfield, and red channels. Epithelium=e. Scale bar = 20 μm.

Genotype	Alpha-Smooth Muscle Actin			Collagen Type III		
	Epi	**Stroma**	**Endo**	**Epi**	**Stroma**	**Endo**
CD-1	1/3	0/3	0/3	3/3	1/3	0/3
CD-1	2/3	1/3	0/3	3/3	0/3	1/3
CD-1	2/2*	0/2*	0/2*	2/2*	0/2*	0/2*
Sey^{neu}	3/3	3/3	0/3	3/3	2/3	0/3
Sey^{neu}	3/3	3/3	0/3	3/3	2/3	0/3
Sey^{neu}	3/3	3/3	3/3	3/3	3/3	1/3

Table 7: Expression of α-smooth muscle actin and collagen type III in 40+ week old wild-type and *Sey*^{neu} mouse corneas. Three sections per sample for each treatment were observed for expression in each layer of the cornea. Epithelium=Epi, endothelium=Endo. *Due to errors in tissue processing, only two samples for this particular treatment for this sample could be included in our study.

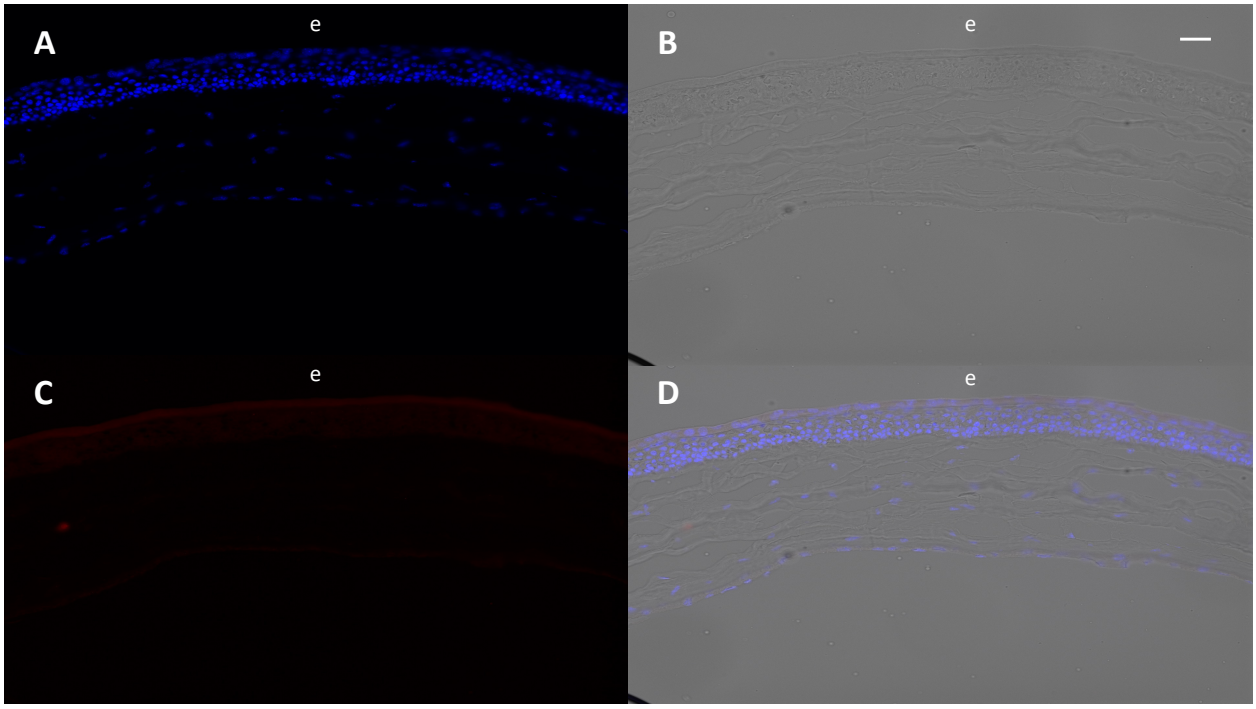

Figure 13: Presence of α-smooth muscle actin in the central cornea of 40+ week old wild-type mouse. (A) 40X image in DAPI channel showing nuclear staining. (B) 40X image in brightfield channel. (C) 40X image in red channel showing α-smooth muscle actin expression. (D) 40X merged image of DAPI, brightfield, and red channels. Epithelium=e. Scale bar = 20 μm.

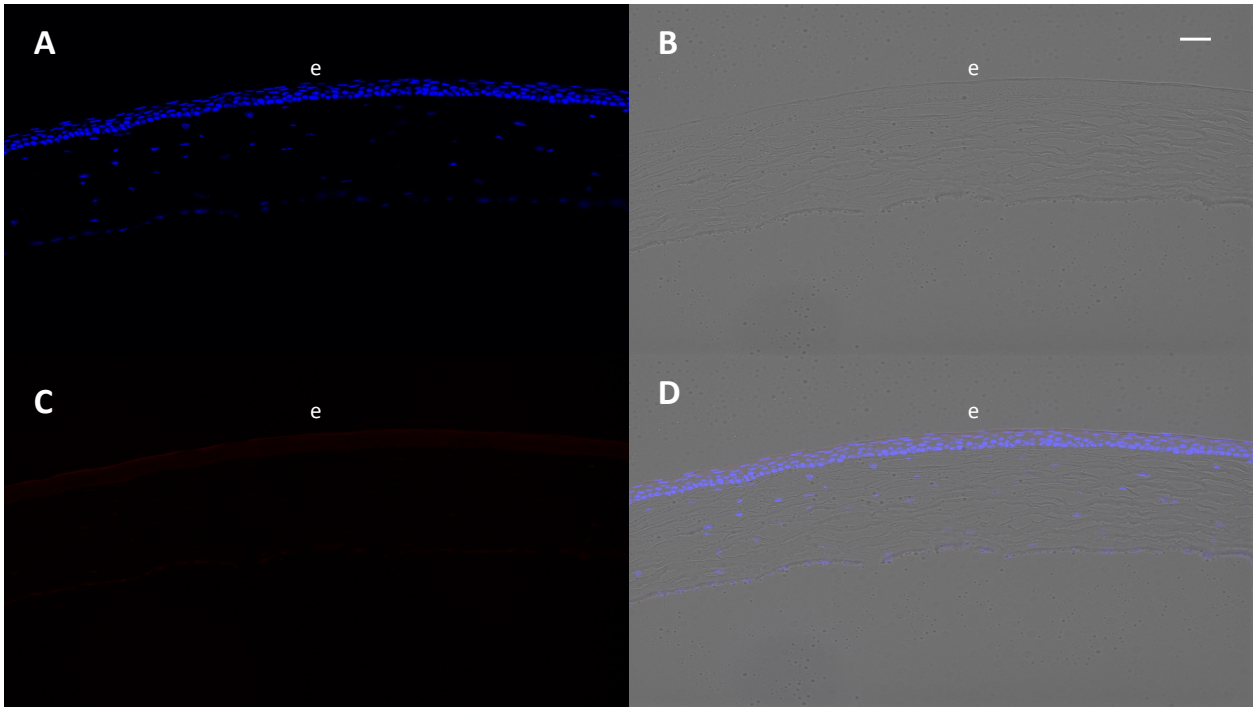

Figure 14: Presence of collagen type III in the central cornea of 40+ week old wild-type mouse. (A) 40X image in DAPI channel showing nuclear staining. (B) 40X image in brightfield channel. (C) 40X image in red channel showing collagen type III expression. (D) 40X merged image of DAPI, brightfield, and red channels. Epithelium=e. Scale bar = 20 μm.

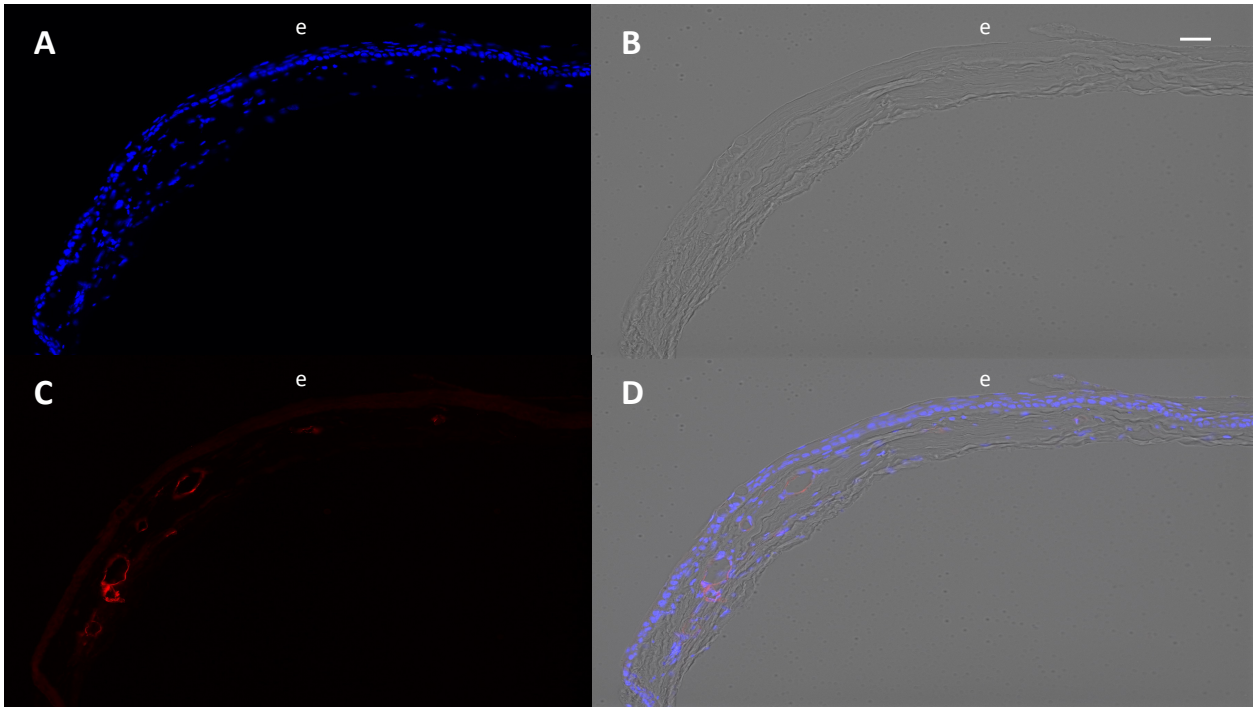

Figure 15: Presence of α-smooth muscle actin in the central cornea of 40+ week old *Sey*^{neu} mouse. (A) 40X image in DAPI channel showing nuclear staining. (B) 40X image in brightfield channel. (C) 40X image in red channel showing α-smooth muscle actin expression. (D) 40X merged image of DAPI, brightfield, and red channels. Epithelium=e. Scale bar = 20 μm.

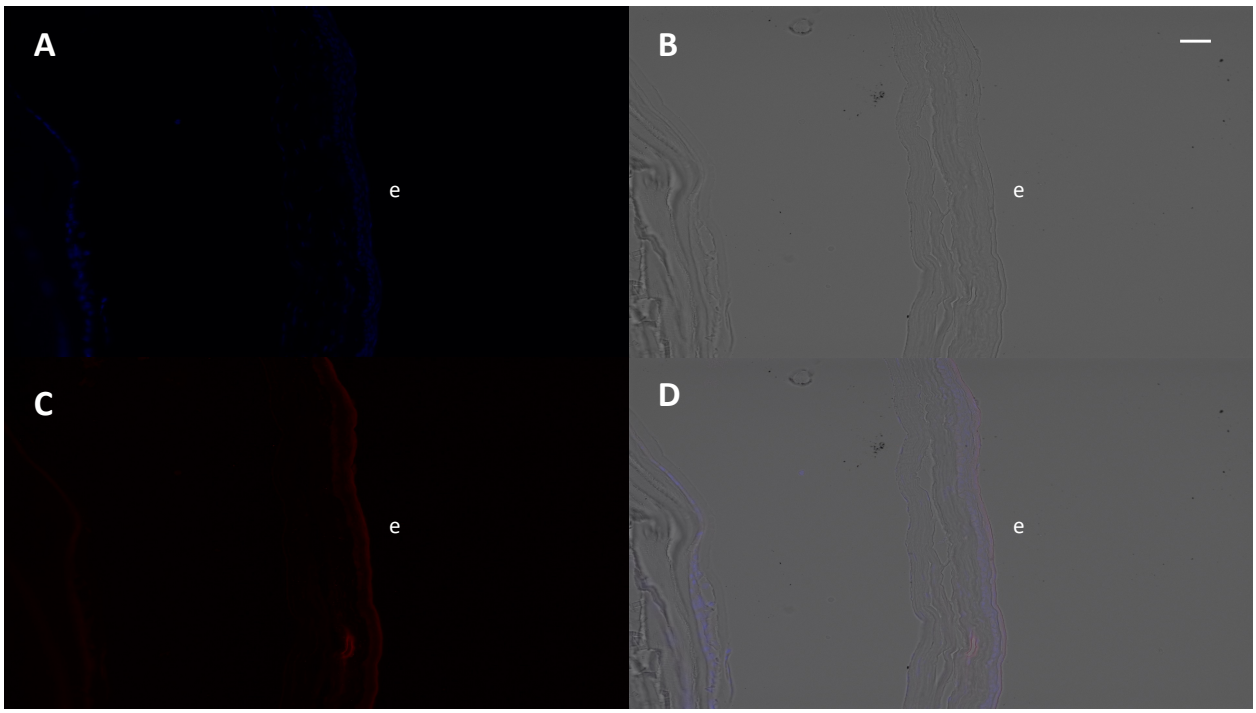

Figure 16: Presence of collagen type III in the central cornea of 40+ week old *Sey*^{neu} mouse. (A) 40X image in DAPI channel showing nuclear staining. (B) 40X image in brightfield channel. (C) 40X image in red channel showing collagen type III expression. (D) 40X merged image of DAPI, brightfield, and red channels. Epithelium=e. Scale bar = 20 μm.

Presence of Alpha-Smooth Muscle Actin				
Age Group	**Genotype**	**Epithelium**	**Stroma**	**Endothelium**
17-19 Weeks	Wild-type (CD-1)	2/5	0/5	0/5
17-19 Weeks	Sey^{neu}	2/3	3/3	2/3
40+ Weeks	Wild-type (CD-1)	3/3	1/3	0/3
40+ Weeks	Sey^{neu}	3/3	3/3	1/3

Table 8: Summary of expression of α-SMA by age group (17-19 weeks old and 40+ weeks old) and genotype (wild-type and *Sey*^{neu}). Quantities represent how many samples expressed α-SMA per age group and genotype.

Presence of Collagen Type III				
Age Group	**Genotype**	**Epithelium**	**Stroma**	**Endothelium**
17-19 Weeks	Wild-type (CD-1)	4/5	0/5	0/5
17-19 Weeks	Sey^{neu}	3/3	1/3	0/3
40+ Weeks	Wild-type (CD-1)	3/3	1/3	1/3
40+ Weeks	Sey^{neu}	3/3	3/3	1/3

Table 9: Summary of expression of Collagen Type III by age group (17-19 weeks old and 40+ weeks old) and genotype (wild-type and *Sey*^{neu}). Quantities represent how many samples expressed Collagen Type III per age group and genotype.

CHAPTER 3

DISCUSSION AND FUTURE DIRECTIONS

3.1 Discussion

The current study has investigated three hypotheses as to what is contributing to corneal clouding in aniridia-related keratopathy (ARK). Specifically, the hypotheses of ocular surface integrity, conjunctivalization, and fibrosis were tackled in this study. Wild-type (*Pax6*$^{+/+}$) and *Sey* (*Pax6*$^{+/-}$) mice were evaluated at time of mild symptoms of ARK (17-19 weeks old) and severe symptoms of ARK (40+ weeks old) as outlined by previous literature[28,30]. Corneal clouding and ocular surface integrity were assessed via clinical evaluation along with fluorescein uptake. Conjunctivalization was investigated through histological evaluation of goblet cells. The pro-fibrotic response was studied through immunofluorescent expression of α-SMA and collagen type III.

Scoring of the clinical symptoms of ARK had not been previously performed in *Sey* mice. Clinical evaluation revealed decreased corneal clarity in *Sey* compared to wild-type in both the earlier and later time points. Corneal clarity further decreased in 40+ week old *Sey* mice as compared to 17-19 week old *Sey* mice. Fluorescein uptake negatively correlated with corneal clouding: as corneal clarity decreased, fluorescein uptake typically increased. Fluorescein uptake is indicative of epithelial cell damage in the cornea, so damage to the corneal epithelium in *Sey* seems to correlate with corneal opacification. These findings are supported by current scoring of ARK in human aniridia, where increased fluorescein uptake is used as an indicator of severity of ARK symptoms[21,28].

Conjunctivalization, or goblet cell infiltration, is commonly taken as an indicator of limbal stem cell deficiency(LSCD). Corneal abnormalities seen in aniridia has been widely hypothesized to be due to LSCD. Conjunctivalization has been recorded in both human and *Sey*[21,30]. If goblet cells entering the cornea contribute to corneal clouding, conjunctivalization should increase as corneal opacification increases. In the current study, goblet cells were increased in Sey corneas compared to wild-type corneas at both time points. 17-19 week old *Sey* mice had more goblet cells than 40+ week old *Sey* mice, contrary to previous findings[30]. During clinical evaluation, corneal clouding was found to increase with age. Therefore, conjunctivalization negatively correlates with corneal opacification; as corneal clouding increased, presence of goblet cells decreased. These findings contradict the prevailing hypothesis of LSCD, providing evidence that LSCD is not the only factor at play in progression of corneal clouding seen in ARK.

The pro-fibrotic response has been shown to reduce transparency of the cornea. Disruption of the EBM allows activation of myofibroblasts, which are less transparent than their keratocyte counterpart[15]. Once myofibroblasts fully mature, disordered ECM is deposited which further reduces transparency[15]. This action has been investigated in the context of infection and surgery[11,16]. The current study has now added the context of *Pax6* deficiency by investigating the pro-fibrotic response in *Sey* mice .

In our study, α-SMA and collagen type III were expressed in low levels in the epithelium of a majority of mice, regardless of age and genotype. At both time points, *Sey* mice showed α-SMA expression in the stroma and endothelium that was not present in wild-type. Collagen type III expression was present in the stroma in some *Sey* mice at the earlier time point, but this stromal expression increased in the older time point. This expression pattern implies that

myofibroblasts are maturing as symptoms of ARK progress. This study has provided new evidence that progressive corneal opacification seen in ARK could be due to increased presence of myofibroblasts that deposit disordered ECM components.

As human aniridia is a pan-ocular condition, there are several potential factors in ARK and corneal opacification, so several mechanisms for corneal clouding in ARK are possible. First is the widely popular limbal stem cell deficiency (LSCD). While LSCD was not directly investigated in this study due to lack of definitive markers, conjunctivalization is taken as an indirect way to judge LSCD. *Sey* mice have shown conjunctivalization in this study, yet it negatively correlated as corneal clouding progressed. Goblet cells most likely are not directly contributing to corneal clouding in *Sey*. Possibly, LSCD has more of an impact in earlier stages of ARK, causing conjunctivalization to occur to compensate for epithelial cell loss. Once late stage ARK has set in from other contributing factors, LSCD plays less of a role and goblet cell infiltration decreases.

Another possibility is that LSCD is more detrimental in human than in a mouse model. When clinically evaluating the *Sey* mice, corneal clouding typically began in the central cornea, then encompassed the central and peripheral cornea as clouding progressed. In some cases of human aniridia, clouding was located more peripherally than centrally[40]. More severe LSCD in humans could cause more goblet cells to be recruited to the peripheral cornea, causing clouding. Clouding that begins more peripherally could be more involved with LSCD than clouding that starts centrally.

Another possible mechanism is a chronic wound healing response, activating fibrosis which reduces transparency. As mentioned previously, the corneal epithelium is reduced in aniridia. The underlying EBM is essential to preventing a pro-fibrotic response from activating in

the stroma. With a thinner epithelium, injury to the cornea may be more likely to disrupt the EBM and trigger fibrosis. In some cases, EBM has even been cited as obliterated or altered in aniridia, so if that barrier is not present, nothing is preventing corneal fibrosis from occurring. Furthermore, if the EBM is altered in aniridia, the fibrotic response may not be able to be inhibited by IL-1, so myofibroblasts are able to fully mature and deposit disordered ECM. In our study, the EBM could not be properly visualized, so integrity of the EBM is uncertain. However, we have shown that a pro-fibrotic response is occurring in *Sey* that increases as corneal clouding increases, so the possibility of EBM disruption is likely.

One unexpected finding from this study points to a mechanism unrelated to injury or LSCD. During immunofluorescent evaluation of the pro-fibrotic response, *Sey* mice occasionally had α-SMA expression in the endothelium. While this expression pattern was not present in all *Sey* samples, it was not found in any capacity in wild-type corneas at any time point. Histologically, this single cell layer appears normal in *Sey* mice. Developmentally, the stroma and endothelium are derived from neural crest cells, a different cell population than corneal epithelium. The *Pax6* gene is thought to primarily be involved in corneal epithelial development and maintenance, but not implicated in development of the endothelium[41]. A possible downstream target of *Pax6* may be involved in endothelial development or maintenance that could be contributing to the pro-fibrotic response seen in *Sey*. Alternatively, structural changes caused by *Pax6* deficiency could be indirectly compromising the health of the corneal endothelium. Iris hypoplasia could be causing irregular flow of aqueous humor on the endothelium, resulting in endothelial cell breakdown and inefficient transport of H_2O and nutrients to the stroma. The role of *Pax6* deficiency in the function of corneal endothelium and its impact on ARK could be an interesting avenue to explore.

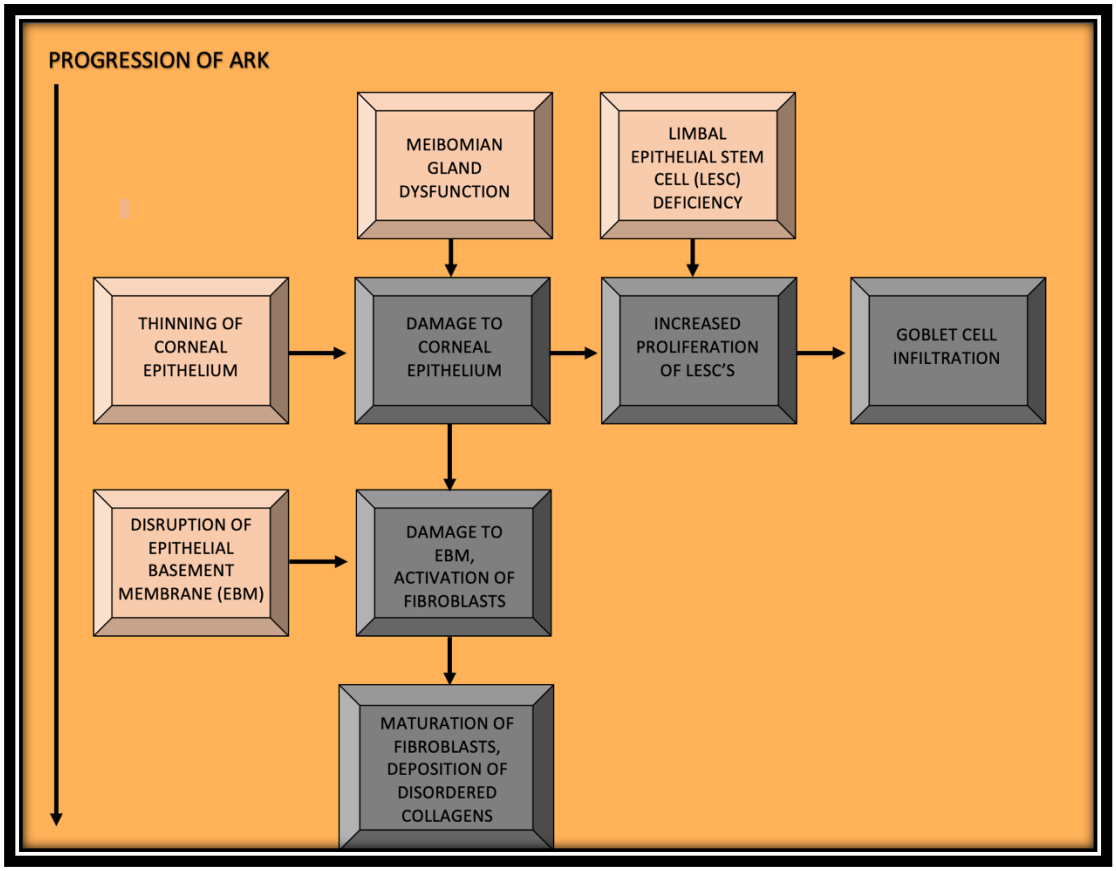

Figure 17: Proposed mechanism for the progression of corneal clouding in aniridia-related keratopathy (ARK). Orange boxes represent structural changes due to *Pax6* deficiency. Grey boxes represent changes in the cornea during ARK. In earlier stages of ARK, meibomian gland dysfunction and thin corneal epithelium increase the likelihood of damage to the corneal epithelium. Epithelial damage as well as limbal stem cell deficiency (LSCD) lead to increased proliferation of limbal epithelial stem cells, which triggers infiltration of goblet cells from the conjunctiva. Therefore, early stage clouding in ARK is primarily due to conjunctivalization. In later stages of ARK, damage to the epithelium, as well as an already fragile epithelial basement membrane, cause the pro-fibrotic response to occur. This cycle of damage and fibrosis continues and corneal clouding progresses over time.

3.2 Future Directions

While the current study has shed some light on potential causes of corneal clouding in ARK, further work needs to be done to definitively determine the mechanism behind corneal clouding. The first step would be repeating the current study's techniques of fluorescein uptake and immunofluoresecent evaluation in a much earlier time point in wild-type and *Sey* mice, around the time of eye opening. Investigating ocular surface integrity and the pro-fibrotic response before the onset of ARK symptoms could help tease apart features that are inherent to *Sey* versus features stemming from ARK. If ocular surface changes and corneal fibrosis is seen in this young time point before corneal clouding has occurred, our findings could be due to intrinsic changes in *Sey* due to *Pax6* deficiency. However, if increased fluorescein uptake and pro-fibrotic markers are not present in this young time point, that would further solidify that our findings are most likely due to progression of ARK.

As mentioned previously, the EBM is a key player in the activation and inhibition of corneal fibrosis. Unfortunately, the EBM cannot be definitively visualized via histology or other methods used in this study, so the integrity of the EBM could not be determined. However, the EBM can be visualized through other means, including transmission electron microscopy. In future studies, the EBM could be characterized through transmission electron microscopy in wild-type and *Sey* mice at time points capturing progression of ARK symptoms. This technique could aid in fully capturing the integrity of the EBM and its potential role in corneal opacification.

While our pro-fibrotic markers utilized in this study captured a scope of myofibroblast development, more markers are known to exist that fully capture a signature of maturity of myofibroblasts. While our use of α-SMA as a marker captures intermediate and mature

myofibroblasts, we did not use a marker that could distinguish between them. Desmin is an intermediate filament protein that is known to be negative in immature myofibroblasts, but positively expressed once they reach full maturity. Future studies could include the use of vimentin and desmin along with α-SMA to fully capture the signature of myofibroblast development as symptoms of ARK progress.

As discussed previously, current treatment methods for ARK are insufficient, thus new avenues of treatment must be explored. The current study has brought new evidence forward that a pro-fibrotic response may be involved in corneal opacification associated with ARK. This new evidence can open up exploration of new treatment methods for ARK. Particularly, existing treatment methods known to be involved in the TGFβ-mediated fibrotic response could be utilized in future studies. For example, intercellular protein MG-53 has been investigated in corneal wound healing, and has been shown to modulate TGFβ-dependent fibrosis[42]. This protein could be applied to a *Pax6* deficient model such as *Sey* and determine if rescue of corneal opacity in ARK is possible. TGFβ is essential for various biological processes in the body, including inflammation and wound repair, so a topical rather than systemic target of TGFβ-mediated fibrosis could be a promising treatment method for ARK.

REFERENCES

1. Sridhar M. S. (2018). Anatomy of cornea and ocular surface. *Indian journal of ophthalmology*, *66*(2), 190–194. https://doi.org/10.4103/ijo.IJO_646_17
2. Eghrari, A. O., Riazuddin, S. A., & Gottsch, J. D. (2015). Overview of the Cornea: Structure, Function, and Development. Progress in molecular biology and translational science, 134, 7–23. https://doi.org/10.1016/bs.pmbts.2015.04.001
3. Fore J. (2006). A review of skin and the effects of aging on skin structure and function. Ostomy/wound management, 52(9), 24–37.
4. Asimellis, G., & Kaufman, E. J. (2020). Keratoconus. In StatPearls. StatPearls Publishing.
5. Meek, K. M., & Knupp, C. (2015). Corneal structure and transparency. Progress in retinal and eye research, 49, 1–16. https://doi.org/10.1016/j.preteyeres.2015.07.001
6. West, J. D., Dorà, N. J., & Collinson, J. M. (2015). Evaluating alternative stem cell hypotheses for adult corneal epithelial maintenance. World journal of stem cells, 7(2), 281–299. https://doi.org/10.4252/wjsc.v7.i2.281
7. Thoft, R. A., & Friend, J. (1983). The X, Y, Z hypothesis of corneal epithelial maintenance. Investigative ophthalmology & visual science, 24(10), 1442–1443.
8. de Oliveira, R. C., & Wilson, S. E. (2020). Fibrocytes, Wound Healing, and Corneal Fibrosis. Investigative ophthalmology & visual science, 61(2), 28. https://doi.org/10.1167/iovs.61.2.28

9. Wilson, S. E. (2020). Corneal wound healing. Experimental Eye Research, 108089. doi:10.1016/j.exer.2020.108089
10. Kao, W. W., & Liu, C. Y. (2010). Corneal morphogenesis during development and wound healing. Japanese journal of ophthalmology, 54(3), 206–210. https://doi.org/10.1007/s10384-010-0800-6
11. Wilson, S. E., Torricelli, A., & Marino, G. K. (2020). Corneal epithelial basement membrane: Structure, function and regeneration. Experimental eye research, 194, 108002. https://doi.org/10.1016/j.exer.2020.108002
12. Medeiros, C. S., Marino, G. K., Santhiago, M. R., & Wilson, S. E. (2018). The Corneal Basement Membranes and Stromal Fibrosis. Investigative ophthalmology & visual science, 59(10), 4044–4053. https://doi.org/10.1167/iovs.18-24428
13. Torricelli, A. A., Santhanam, A., Wu, J., Singh, V., & Wilson, S. E. (2016). The corneal fibrosis response to epithelial-stromal injury. Experimental eye research, 142, 110–118. https://doi.org/10.1016/j.exer.2014.09.012
14. Massoudi, D., Malecaze, F., & Galiacy, S. D. (2016). Collagens and proteoglycans of the cornea: importance in transparency and visual disorders. Cell and tissue research, 363(2), 337–349. https://doi.org/10.1007/s00441-015-2233-5
15. Wilson, S. E., Marino, G. K., Torricelli, A., & Medeiros, C. S. (2017). Injury and defective regeneration of the epithelial basement membrane in corneal fibrosis: A paradigm for fibrosis in other organs?. Matrix biology : journal of the International Society for Matrix Biology, 64, 17–26. https://doi.org/10.1016/j.matbio.2017.06.003

16. Wilson S. E. (2012). Corneal myofibroblast biology and pathobiology: generation, persistence, and transparency. Experimental eye research, 99(1), 78–88. https://doi.org/10.1016/j.exer.2012.03.018
17. Aniridia. Bioetymology. https://bioetymology.blogspot.com/2018/06/aniridia.html
18. Hingorani, M., Hanson, I., & van Seyningen, V. (2012). Aniridia. European journal of human genetics : EJHG, 20(10), 1011–1017. https://doi.org/10.1038/ejhg.2012.100
19. Singh, V., Torricelli, A. A., Nayeb-Hashemi, N., Agrawal, V., & Wilson, S. E. (2013). Mouse strain variation in SMA(+) myofibroblast development after corneal injury. Experimental eye research, 115, 27–30. https://doi.org/10.1016/j.exer.2013.06.006
20. Godavová, L., Godava, M., Sabová, J., Kolářová, G., & Mohlerová, S. (2014). Klinické nálezy u členů rodiny s výskytem izolované aniridie v důsledku PAX6 mutace [Clinical Findings in Family with Aniridia due the PAX6 Mutation]. Ceska a slovenska oftalmologie : casopis Ceske oftalmologicke spolecnosti a Slovenske oftalmologicke spolecnosti, 70(4), 138–144.
21. Samant, M., Chauhan, B. K., Lathrop, K. L., & Nischal, K. K. (2016). Congenital aniridia: etiology, manifestations and management. Expert review of ophthalmology, 11(2), 135–144. https://doi.org/10.1586/17469899.2016.1152182
22. Onuma, Y., Takahashi, S., Asashima, M., Kurata, S., & Gehring, W. J. (2002). Conservation of Pax 6 function and upstream activation by Notch signaling in eye development of frogs and flies. Proceedings of the National Academy of Sciences of the United States of America, 99(4), 2020–2025. https://doi.org/10.1073/pnas.022626999

23. Jones, L., López-Bendito, G., Gruss, P., Stoykova, A., & Molnár, Z. (2002). Pax6 is required for the normal development of the forebrain axonal connections. Development (Cambridge, England), 129(21), 5041–5052.

24. Favor, J., Bradley, A., Conte, N., Janik, D., Pretsch, W., Reitmeir, P., Rosemann, M., Schmahl, W., Wienberg, J., & Zaus, I. (2009). Analysis of Pax6 contiguous gene deletions in the mouse, Mus musculus, identifies regions distinct from Pax6 responsible for extreme small-eye and belly-spotting phenotypes. Genetics, 182(4), 1077–1088. https://doi.org/10.1534/genetics.109.104562

25. Lima Cunha, D., Arno, G., Corton, M., & Moosajee, M. (2019). The Spectrum of PAX6 Mutations and Genotype-Phenotype Correlations in the Eye. Genes, 10(12), 1050. https://doi.org/10.3390/genes10121050

26. Wang, X., Shan, X., & Gregory-Evans, C. Y. (2017). A mouse model of aniridia reveals the *in vivo* downstream targets of Pax6 driving iris and ciliary body development in the eye. Biochimica et biophysica acta. Molecular basis of disease, 1863(1), 60–67. https://doi.org/10.1016/j.bbadis.2016.10.018

27. van Seyningen, V., & Williamson, K. A. (2002). PAX6 in sensory development. Human molecular genetics, 11(10), 1161–1167. https://doi.org/10.1093/hmg/11.10.1161

28. Yazdanpanah, G., Bohm, K. J., Hassan, O. M., Karas, F. I., Elhusseiny, A. M., Nonpassopon, M., Niparugs, M., Tu, E. Y., Sugar, J., Rosenblatt, M. I., Cortina, M. S., & Djalilian, A. R. (2020). Management of Congenital Aniridia-Associated Keratopathy: Long-Term Outcomes from a Tertiary Referral Center. American journal of ophthalmology, 210, 8–18. https://doi.org/10.1016/j.ajo.2019.11.003

29. Whitson, J. T., Liang, C., Godfrey, D. G., Petroll, W. M., Cavanagh, H. D., Patel, D., Fellman, R. L., & Starita, R. J. (2005). Central corneal thickness in patients with congenital aniridia. Eye & contact lens, 31(5), 221–224. https://doi.org/10.1097/01.icl.0000152487.16012.40

30. Ramaesh, T., Collinson, J. M., Ramaesh, K., Kaufman, M. H., West, J. D., & Dhillon, B. (2003). Corneal abnormalities in Pax6+/- small eye mice mimic human aniridia-related keratopathy. Investigative ophthalmology & visual science, 44(5), 1871–1878. https://doi.org/10.1167/iovs.02-0576

31. Margo C. E. (1983). Congenital aniridia: a histopathologic study of the anterior segment in children. Journal of pediatric ophthalmology and strabismus, 20(5), 192–198.

32. Radhakrishnan, S., & Iwach, A. (2016, September 16). Glaucoma Medications and their Side Effects. Glaucoma Research Foundation. https://www.glaucoma.org/gleams/glaucoma-medications-and-their-side-effects.php

33. Burk, S. E., Da Mata, A. P., Snyder, M. E., Cionni, R. J., Cohen, J. S., & Osher, R. H. (2001). Prosthetic iris implantation for congenital, traumatic, or functional iris deficiencies. Journal of cataract and refractive surgery, 27(11), 1732–1740. https://doi.org/10.1016/s0886-3350(01)01124-5

34. Le, Q., Deng, S. X., & Xu, J. (2013). *In vivo* confocal microscopy of congenital aniridia-associated keratopathy. Eye (London, England), 27(6), 763–766. https://doi.org/10.1038/eye.2013.50

35. Edén, U., Riise, R., & Tornqvist, K. (2010). Corneal involvement in congenital aniridia. Cornea, 29(10), 1096–1102. https://doi.org/10.1097/ICO.0b013e3181d20493

36. Davis, J., Duncan, M. K., Robison, W. G., Jr, & Piatigorsky, J. (2003). Requirement for Pax6 in corneal morphogenesis: a role in adhesion. Journal of cell science, 116(Pt 11), 2157–2167. https://doi.org/10.1242/jcs.00441

37. Holland, E. J., Djalilian, A. R., & Schwartz, G. S. (2003). Management of aniridic keratopathy with keratolimbal allograft: a limbal stem cell transplantation technique. Ophthalmology, 110(1), 125–130. doi:10.1016/s0161-6420(02)01451-3

38. Hassanaly, S. I., Talajic, J. C., & Harissi-Dagher, M. (2014). Outcomes Following Boston Type 1 Keratoprosthesis Implantation in Aniridia Patients at the University of Montreal. American Journal of Ophthalmology, 158(2), 270–276.e1. doi:10.1016/j.ajo.2014.05.009

39. Boston Keratoprosthesis (KPro). EyeWiki. (2021, April 6). https://eyewiki.aao.org/Boston_Keratoprosthesis_(KPro).

40. Vicente, A., Byström, B., Lindström, M., Stenevi, U., & Pedrosa Domellöf, F. (2018). Aniridia-related keratopathy: Structural changes in naïve and transplanted corneal buttons. PloS one, 13(6), e0198822. https://doi.org/10.1371/journal.pone.0198822

41. Park, J. W., Yang, J., & Xu, R. H. (2018). PAX6 Alternative Splicing and Corneal Development. Stem cells and development, 27(6), 367–377. https://doi.org/10.1089/scd.2017.0283

42. Chandler, H. L., Tan, T., Yang, C., Gemensky-Metzler, A. J., Wehrman, R. F., Jiang, Q., Peterson, C., Geng, B., Zhou, X., Wang, Q., Kaili, D., Adesanya, T., Yi, F., Zhu, H., & Ma, J. (2019). MG53 promotes corneal wound healing and mitigates fibrotic remodeling in rodents. Communications biology, 2, 71. https://doi.org/10.1038/s42003-019-0316-7

APPENDIX

A. Detailed Fluorescein Uptake Protocol

Fluorescein Uptake Protocol

Materials

- Fluorescein solution**
- Rewetting drops
- Mice/animal of interest
- 4% PFA

Equipment

- Euthanasia chamber
- Surgical pads
- Tape
- Pipette with tips (100 ul and 1 ml)
- Kim wipes
- Stereo Microscope with Brightfield and FITC 480 filter settings
- 1.5 ml tubes
- Small scissors
- forceps

Setting Up the Procedure Area

- Turn on stereo microscope and fluorescent X-Cite equipment (*fluorescent equipment must be kept on for a minimum of 30 minutes)
- Use a large surgical pad to cover the work area surface, tape down to prevent it from sliding
- Use a smaller square of a surgical pad to cover the center of the work area above the microscope and tape into place. This will catch any residual fluorescein or rewetting drops (change out for clean surgical pad as needed)
- Set your pipettes, tips, rewetting drops, Kim wipes, and prepared fluorescein solution* next to your work area
- Place 1ml of 4% PFA in 1.5ml tubes (one for each eye), set next to work area

Procedure

- **Euthanize the animal:** Place one animal in euthanasia chamber, turn on CO_2 at 1.0L/min. Wait 60 seconds after last inhalation to remove animal from chamber. Always perform a secondary measure of euthanasia before continuing (ex: cervical dislocation)
- Place 100-200 microliters of rewetting drops onto the ocular surface, wait 30 seconds to give the solution time to absorb. Keep ocular surface moisturized throughout procedure
- (Optional) Using small pair of scissors, carefully cut whiskers of animal to avoid them getting in the way of images
- Use exam sheet to assess presence of iris, corneal clarity, lens clarity, and lens placement
- Take images of eye in brightfield and FITC 480 filter before fluorescein application
- Place 100 microliters of fluorescein solution onto the ocular surface. Allow fluorescein to absorb for 60 seconds
- Remove fluorescein by thoroughly washing eye with rewetting drops
- Use exam sheet to assess ocular surface integrity, and draw areas of fluorescein uptake
- Take image in FITC 480 filter post-fluorescein application
- When finished taking images, carefully enucleate eye with forceps and place in tube with 4% PFA
- Repeat process with contralateral eye

B. Clinical Evaluation Exam Sheet

Date:_____ Time:_____ Initials:____

Genotype:_____ ID:_____ DOB:_____ Sex:_____

Notes/Comments:_____

_____

_____

_____

OD	OS
Iris: ○ Present ○ Partially Present ○ Absent ○ Unable to Determine	**Iris:** ○ Present ○ Partially Present ○ Absent ○ Unable to Determine
Lens Clarity: ○ 0 ○ 1 ○ 2 ○ 3	**Lens Clarity:** ○ 0 ○ 1 ○ 2 ○ 3
Corneal Clarity: ○ 0 ○ 1 ○ 2 ○ 3	**Corneal Clarity:** ○ 0 ○ 1 ○ 2 ○ 3
Lens Placement: ○ 0 ○ 1	**Lens Placement:** ○ 0 ○ 1
Ocular Surface Integrity: ○ 0 ○ 1 ○ 2 ○ 3	**Ocular Surface Score:** ○ 0 ○ 1 ○ 2 ○ 3

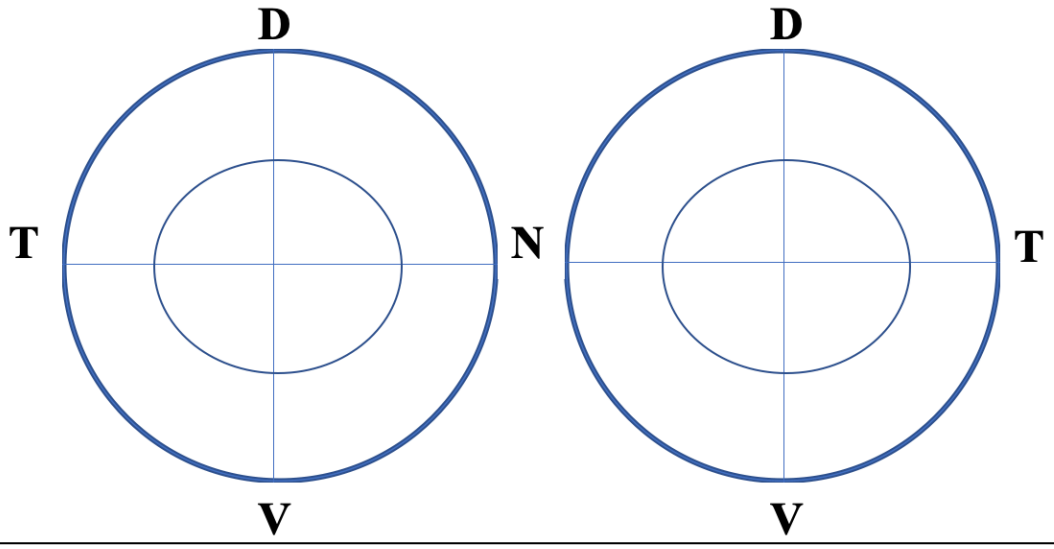

C. Clinical Evaluation Scoring Rubrics

Lens Clarity:

Score	Presentation
0	Lens is completely transparent.
1	Lens has slight haze on either periphery or center.
2	Lens has slight haze to periphery and center.
3	Lens is completely opaque.

Lens Placement:

Score	Presentation
0	Lens is well-centered and positioned directly posterior and deep to the iris.
1	Lens is not well-centered, and/or is not positioned directly posterior and deep to the iris

Corneal Clarity:

Score	Presentation
0	Cornea is completely transparent, iris detail and pupil are clearly visible.
1	Cornea is completely opaque in periphery of at least one quadrant, becoming translucent in periphery of at least three out of four quadrants. Center of all four quadrants is clear. Iris detail less visible, pupil still clearly visible.
2	Cornea is completely opaque in periphery of at least three out of four quadrants, center of at least one quadrant is translucent. Iris detail and pupil less visible.
3	Cornea is completely opaque in periphery and center of at least three out of four quadrants. Iris detail is lost, pupil not clearly visible.

Ocular Surface Integrity:

Score	Presentation
0	No fluorescein uptake detected, ocular surface is free of signs of trauma.
1	Fluorescein uptake detected in at least one quadrant, OR punctate uptake detected in two to three quadrants of ocular surface.
2	Fluorescein uptake detected in larger than punctate amount in two to three quadrants, OR over half of one quadrant of ocular surface.
3	Uptake of fluorescein detected in at least half of all four quadrants of ocular surface.

D. Examples of Clinical Evaluation Exam Sheet

Example 1:

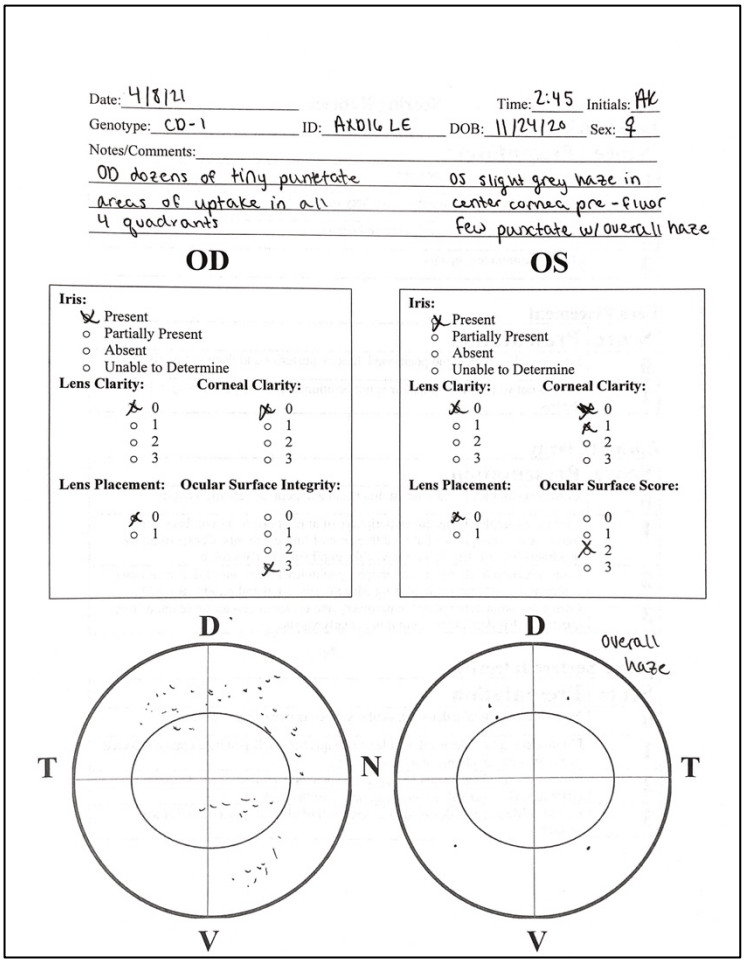

Example 2:

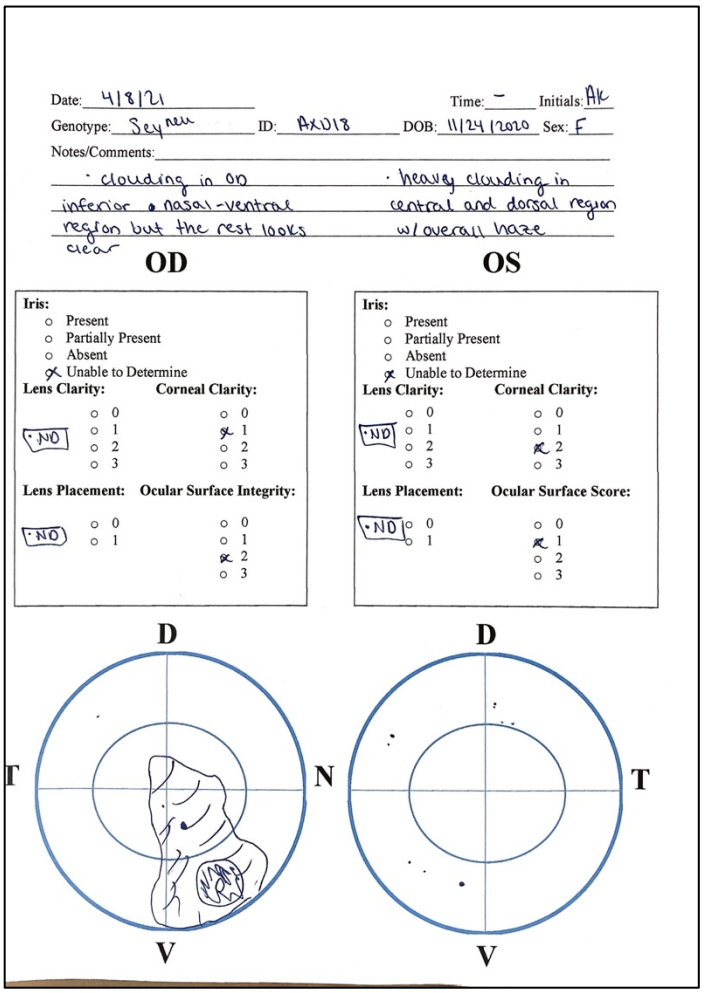

Date: 4/8/21 Time: – Initials: AK

Genotype: Seynew ID: AX018 DOB: 11/24/2020 Sex: F

Notes/Comments:

OD: · clouding in OD inferior • nasal-ventral region but the rest looks clear

OS: · heavy clouding in central and dorsal region w/ overall haze

OD

Iris:
- ○ Present
- ○ Partially Present
- ○ Absent
- ☒ Unable to Determine

Lens Clarity: ND — ○ 0 ○ 1 ○ 2 ○ 3

Corneal Clarity: ○ 0 ☒ 1 ○ 2 ○ 3

Lens Placement: ND — ○ 0 ○ 1

Ocular Surface Integrity: ○ 0 ○ 1 ☒ 2 ○ 3

OS

Iris:
- ○ Present
- ○ Partially Present
- ○ Absent
- ☒ Unable to Determine

Lens Clarity: ND — ○ 0 ○ 1 ○ 2 ○ 3

Corneal Clarity: ○ 0 ○ 1 ☒ 2 ○ 3

Lens Placement: ND — ○ 0 ○ 1

Ocular Surface Score: ○ 0 ☒ 1 ○ 2 ○ 3